An NKX2-5 homolog is required downstream of BMP signaling to pattern the sensory-adhesive organ of a tunicate larva

Christopher J. Johnson[1]*, Joshua Kavaler[2], Christina D. Cota[2], Alberto Stolfi[1]*

1. School of Biological Sciences, Georgia Institute of Technology, Atlanta, GA, USA
2. Biology Department, Colby College, Waterville, Maine, USA
* cvjohnson1215@gatech.edu, alberto.stolfi@biosci.gatech.edu

ABSTRACT

Tunicates are the sister group to vertebrates within the chordate phylum, yet unlike other chordate groups, they evolved a biphasic lifecycle alternating between motile larvae and sessile adults. The papillae of most tunicate larvae are the key sensory-adhesive organ regulating their settlement and metamorphosis. The papillae are nearly always arranged as a group of three morphologically identical organs that arise from an anterior neural plate border region nested between ventral epidermis and more dorsal/posterior neural tube progenitors. Due to their embryonic origin and molecular signatures, this anterior border has been evolutionarily linked to vertebrate placode regions. It was previously shown that the specification, patterning, and morphogenesis of the embryonic papilla region all depend on BMP signaling, though downstream mechanisms remain poorly understood. Here we show that the NKX2-3/5/6 ortholog NK4 is a key transcription factor that acts downstream of BMP signaling to pattern the papillae in the *Ciona* embryo. We present evidence that *NK4* is activated by BMP signaling and encodes a transcriptional repressor that is required to restrict the expression of the papilla regulatory gene *Foxg* to three cell clusters that give rise to the three papillae. Loss of NK4 function results in the formation of a single large papilla. In contrast, overexpression of NK4 represses *Foxg,* eliminating the papillae. We also show that the expression of *NK4* is restricted dorsally by the BMP antagonist Chordin, while the ventrally-expressed transcription factor Msx alleviates the repressive effect of NK4, potentially allowing for the characteristic tripartite patterning of the papillae.

INTRODUCTION

Tunicates have emerged as model organisms for the study of chordate evolution and development (Anselmi et al., 2025). Despite sharing key anatomical, cellular, and molecular traits with other chordate subphyla, a majority of tunicate species alternate between motile, pelagic larval and sessile, benthic adult lifecycle phases (Karaiskou et al., 2015; Lemaire, 2011). The sensory-adhesive papilla organ of the larva plays an indispensable role in driving substrate attachment and metamorphosis in most species (Nakayama-Ishimura et al., 2009). In solitary species studied in the lab, it has been shown that continuous attachment to a solid substrate is necessary and sufficient to trigger metamorphosis (Matsunobu and Sasakura, 2015). This metamorphosis has been shown to be driven by the mechanosensory abilities of the papillae, and direct mechanical or optogenetic stimulation of the papilla neurons (PNs) can substitute for attachment in initiating metamorphosis (Totsuka and Hotta, 2025; Wakai et al., 2021). It is thought that the PNs sense mechanical forces generated and/or augmented by substrate attachment (Hozumi et al., 2025), which in turn depends on adhesive material-secreting collocytes that are present alongside the PNs in the papilla organ (Zeng et al., 2019a; Zeng et al., 2019b). Consistent with this model, metamorphosis is blocked by genetically eliminating PNs or perturbing their function (Sakamoto et al., 2022). In most species, the papilla organ is invariably organized in a tripartite manner, consisting of three constituent papillae arranged as vertices of a triangle: two dorsal, lateral papillae and one ventral, medial papilla (Berrill, 1930; Dolcemascolo et al., 2009; Turon, 1991). Each papilla appears to consist of the same number and arrangement of cell types, of which at least five are known based on cytological and molecular characterization (Johnson et al., 2024; Zeng et al., 2019b). This tripartite arrangement is highly conserved, even in the much larger larvae of certain compound tunicate species (Cloney, 1977), suggesting some adaptive advantage for the larva.

The papillae arise from the anteriormost cells of the neural plate, forming an anterior neural border (ANB) that might be evolutionarily connected to the anterior cranial placodes of vertebrates (Abitua et al., 2015; Feinberg et al., 2019; Ikeda et al., 2013; Liu et al., 2023; Roure et al., 2023; Roure et al., 2025; Thawani and Groves, 2020; Tresser et al., 2010; Wagner and Levine, 2012). In multiple species studied, the specification and patterning of the papilla region is regulated by BMP signaling (Liu et al., 2023; Roure et al., 2023). First, BMP signaling is required for proper papilla specification, though in more anterior/ventral epidermis it may suppress papilla fate (Liu et al., 2023; Roure et al., 2023). Later, BMP signaling patterns the

papilla territory into its familiar tripartite arrangement (Liu et al., 2023; Roure et al., 2023). It has also been shown that the tripartite organization of the papillae depends on the precise specification of three discrete, Foxg+/Islet+ cell clusters at the mid/late tailbud stages (Johnson et al., 2024; Liu and Satou, 2019; Roure et al., 2023; Wagner et al., 2014). However, our understanding of how BMP or other candidate pathways accomplish this remains incomplete (**Figure 1**).

Here we show that the BMP-responsive regulatory gene *Nkx2-3/5/6,* the ortholog of *NKX2-5, NKX2-3,* and *NKX2-6* in humans, and of *tinman* in *Drosophila,* is a key intermediate regulator that mediates the BMP-dependent tripartite patterning of the *Ciona* papillae. We show that BMP signaling in the papilla territory promotes expression of *Nkx2-3/5/6* (which we call *NK4* herein, based on the original name of the *Drosophila* tinman protein, NK-4)(Kim and Nirenberg, 1989). We further show that NK4 acts as a transcriptional repressor that is both necessary and sufficient to downregulate *Foxg* expression in specific sub-regions of this territory, thereby allowing for the formation of discrete *Foxg+* cell clusters that give rise to the three papillae. Disrupting *NK4* largely phenocopies BMP inhibition, resulting in a single large papilla. We discuss our findings in the context of a larger model that we propose as underlying the development of the conserved tripartite organization of the papilla organ, and its implications for larval settlement and metamorphosis.

RESULTS

Knocking out NK4 in the papillae using CRISPR/Cas9 phenocopies BMP inhibition

We initially identified NK4 as a potential regulator of cell fate in the papillae. *NK4* is expressed throughout the papilla territory (**Figure 2A, Figure S1, Video S1**)(Johnson et al., 2020), where it was hypothesized to be important for the specification of the Axial Columnar Cells (ACCs), a papilla cell type with sensory capabilities but of unknown function (Hoyer et al., 2024; Johnson et al., 2020). We thus originally sought to knock out *NK4* specifically in the papilla territory, to assay its role in ACC specification. To do so, we selected a previously designed and validated, high-efficiency single-chain guide RNA (sgRNA) targeting the second exon of *NK4* (**Figure 2B**), predicted to cut within the sequence encoding part the DNA-binding homeodomain (Gandhi et al., 2017). To limit CRISPR/Cas9 activity to the early papilla cell lineages, we used the *Foxc* promoter to drive expression of Cas9 (*Foxc>Cas9*)(Johnson et al., 2024). When we co-electroporated the sgRNA expression plasmid (*U6>NK4.3*) with *Foxc>Cas9,* we unexpectedly

103 observed a "*Cyrano*" phenotype (Roure et al., 2023) in which a single protruding papilla forms in
104 place of the familiar three papillae arranged as a triangle (**Figure 2C,D**). This phenotype was
105 originally observed in larvae subjected to BMP signaling knockdown (Liu et al., 2023; Roure et
106 al., 2023), but to our knowledge this is the first report of a CRISPR condition with the same or
107 similar phenotype. The ACC reporter gene *CryBG>GFP* was still expressed in *NK4* CRISPR
108 larvae showing a clear single-papilla phenotype (**Figure 2C,E**), suggesting that NK4 is
109 specifically involved in papilla organ patterning but not necessarily cell type specification or
110 differentiation. To test this, we replicated the CRISPR-mediated disruption of *NK4* while
111 assaying the expression of reporters that label the other cell types of the papillae (**Figure 3A,B**).
112 Indeed, all cell type reporters were still labeling cells contributing to the resulting single large
113 papilla. The same phenotype of a single large papilla was obtained using another sgRNA
114 targeting a different part of the *NK4* gene, further supporting our observations (**Figure S2**).
115 Despite only having one large papilla, *NK4* CRISPR larvae were still fully capable of undergoing
116 metamorphosis (**Figure 3C,D**), likely due to the fact that all the cell types, especially the PNs,
117 were still present. Of note, PNs in *NK4 CRISPR* larvae still had their apical cilia, which are
118 hypothesized to be important for mechanosensory ability (**Video S2-4**) These results suggest
119 that the tripartite organization of the papillae might not be required for metamorphosis under
120 laboratory conditions, but could be more important for robust adhesion or to fine-tune substrate
121 selection in the wild.
122
123 **BMP signaling activates *NK4* expression in the papilla territory**
124 In *Ciona, NK4* has been shown to be activated by BMP signaling emanating from ventral
125 regions (Christiaen et al., 2010; Roure et al., 2023; Waki et al., 2015). In the migrating
126 cardiopharyngeal progenitors, BMP signaling activates *NK4,* which in turn modulates cell
127 migration and fate decisions in this lineage (Christiaen et al., 2010). In other studies, *NK4*
128 expression in the ventral epidermis was shown to be upregulated by BMP treatment and
129 downregulated by pharmacological inhibitors of the BMP pathway (Roure et al., 2023; Waki et
130 al., 2015). Because the characteristic phenotype originally described in BMP-inhibited larvae so
131 closely resembled that of our *NK4* CRISPR larvae, we reasoned that *NK4* might act
132 downstream of BMP signaling to pattern the papillae.
133
134 To test this, first we showed that overexpression of the BMP antagonist Noggin (*Foxc>Noggin)*
135 also results in a single protruding papilla containing all known papilla cell types (**Figure 4A**).
136 Second, we found that *Foxc>Noggin* also greatly reduces the expression of the *NK4>GFP*

137 reporter plasmid in the papillae (**Figure 4B**). Expression was not completely abolished, but
138 quantification of mean GFP fluorescence (normalized to whole-larva expression of an
139 *Islet>mCherry* reporter) showed that it is significantly reduced upon BMP inhibition (**Figure 4C-**
140 **E, Figure S3**). Interestingly, we observed a complete loss of expression of the the BMP-
141 dependent ventral papilla marker gene *Msx* (Roure et al., 2023) in Noggin-overexpression
142 larvae, compared to a more modest reduction in *NK4* CRISPR larvae (**Figure 4F,G**). Despite
143 the presence of a single large papilla in in many of these larvae, *Msx* reporter plasmid
144 expression was still observed in the ventral area of the papilla region (**Figure 4F**). This
145 suggests that, although NK4 functions downstream of BMP signaling to regulate the tripartite
146 organization of the papillae, activation of *Msx* in the ventral papilla by BMP is mostly
147 independent of NK4.
148
149 In contrast to *NK4* CRISPR or BMP inhibition, overexpression of NK4 (*Foxc>NK4*) resulted in
150 the near opposite of the *Cyrano* phenotype: a flat layer of cells where the papillae normally form
151 (**Figure 4H,I**). When combining NK4 overexpression with BMP inhibition (Noggin
152 overexpression), the NK4 overexpression phenotype (flat/no papillae) clearly prevailed (**Figure**
153 **4J,K**). Taken together, these data suggest that NK4 acts downstream of BMP signaling in the
154 papilla territory to pattern this region into the three protrusions invariably seen in wild-type
155 larvae.
156
157 **NK4 represses *Foxg***
158 Having established a role for NK4 in patterning the papilla organ downstream of BMP signaling,
159 we next sought to better understand exactly how NK4 achieves this. *NK4* expression has been
160 shown to begin during the neurula stage (Imai et al., 2004). By mRNA *in situ* hybridization we
161 observed *NK4* expression in the middle of the papilla territory during the late neurula stage,
162 overlapping with *Foxg* expression when the latter is still expressed in the anteriormost "U"-
163 shaped row of cells in the papilla territory (**Figure 5A**). This is just before the refinement of *Foxg*
164 expression into the three cell clusters, or "spots", corresponding to the future protrusions
165 (**Figure 1**). At the initial tailbud stage, *NK4* appeared to be most strongly expressed in *Foxg*-
166 negative cells surrounding the future papillae, including in *Foxg*+ cells that nonetheless
167 downregulate *Foxg* later on (Liu and Satou, 2019), as well as in cells of the presumptive ventral
168 papilla (**Figure 5A**). *NK4* appears to be expressed at lower levels in more dorsal and lateral
169 regions, especially near the two dorsolateral "spots" of *Foxg* expression corresponding to the
170 two dorsal papillae.

171

172 Due to the fact that Foxg promotes Islet expression, and that both are required for the formation
173 of the three protrusions later on (Liu et al., 2023; Liu and Satou, 2019; Wagner et al., 2014), we
174 hypothesized that NK4 might downregulate *Foxg* in cells between and surrounding the three
175 *Foxg+/Islet+* cell clusters. Indeed, we found that *NK4* CRISPR results in ectopic *Foxg*
176 expression, observed by *in situ* at the mid-tailbud stage (**Figure 5B,C**). Instead of the three
177 characteristic *Foxg+* cell clusters, we observe a "U"-shaped stripe of *Foxg* expression. This
178 phenocopied the expansion of *Foxg* in BMP-inhibited larvae previously reported (Liu et al.,
179 2023; Roure et al., 2023). We further observed that NK4 CRISPR similarly expands Islet
180 reporter expression from three dots to a U-shaped stripe, like the expansion of Islet observed
181 under BMP inhibition (**Figure 5D,E**)(Roure et al., 2023). It is thought that the expansion of these
182 three *Foxg+/Islet+* clusters into a single contiguous group (**Figure 5F**) results in the enlarged
183 protrusion seen in BMP-knockdown larvae (Liu et al., 2023; Roure et al., 2023). Indeed,
184 *Foxg>GFP* reporter expression was observed throughout the single large papillae of *NK4*
185 CRISPR larvae (**Figure 5G**). In contrast, NK4 overexpression (Foxc>NK4) suppressed Foxg
186 reporter expression (**Figure 6A,B**). Taken together, these data suggest that NK4 is necessary
187 and sufficient to repress *Foxg* in the papillae. Curiously, *Foxc>NK4* does not appear to suppress
188 *Islet* reporter expression (**Figure S4**), suggesting more complex regulatory outcomes
189 downstream of Foxg.
190

191 NK4 has a repressive effect, whether directly or indirectly, on *Foxg* expression, and loss of NK4
192 impairs the refinement of *Foxg* expression into three discrete cell clusters. It was previously
193 shown that Foxg overexpression results in a single large papilla protrusion (Liu and Satou,
194 2019). To test whether impaired refinement/downregulation of *Foxg* likely underlies the
195 phenotype seen in BMP inhibition and *NK4* CRISPR conditions, we electroporated a *Foxg>Foxg*
196 plasmid designed to overexpress Foxg and thus override the normal downregulation of *Foxg*.
197 Indeed, the *Foxg>Foxg* plasmid results in a single enlarged papilla with all four major papilla cell
198 types present, similar to both BMP inhibition and *NK4* CRISPR (**Figure 6C**). However, when we
199 co-electroporated the *Foxc>Nk4* and *Foxg>Foxg* plasmids together in the same embryos, a
200 majority of larvae developed a flat papilla territory, more closely resembling the *Foxc>NK4*
201 phenotype (**Figure 6D,E**). This suggests that NK4 is able to suppress Foxg expression and/or
202 function, and downstream papilla formation. Based on these results, we propose that the single,
203 large protruding papilla seen with *NK4* CRISPR is due to impaired downregulation of Foxg in
204 cells outside the three cell clusters that normally give rise to the three papillae.

NK4 and its orthologs in other species have been described as both transcriptional activators and repressors (Akazawa and Komuro, 2005; Choi et al., 1999). To probe whether NK4 is acting as an activator or a repressor in the papilla territory, we replaced the C-terminus of NK4 with either a VP16 transactivation domain (Campbell et al., 1984), or a WRPW repressor domain (Fisher et al., 1996), and expressed either throughout the papilla territory using the *Foxc* promoter. Strikingly, the effects of overexpressing NK4::VP16 appeared similar to the overexpression of Foxg, resulting in a single, large *Foxg*+ papilla (**Figure 6F,G**). In contrast, overexpression of NK4::WRPW phenocopied that of the full-length NK4, resulting instead in a flat papilla territory (**Figure 6H,I**). These data suggest that NK4 normally functions as a transcriptional repressor of *Foxg* expression during papilla morphogenesis.

Msx interferes with NK4-mediated repression of Foxg

While NK4 appears to mediate the downregulation of *Foxg*, we next asked how the ventral, medial protrusion forms. This protrusion arises from an area with high levels of BMP signaling (Roure et al., 2023) and NK4 expression. Indeed, by *in situ* hybridization, strong *NK4* and *Foxg* expression overlap in the ventral/medial papilla (**Figure 5A**), which is known to express *Msx* (**Figure 4F**). We therefore hypothesized that Msx might somehow interfere with NK4's ability to repress *Foxg.* To test this, we co-electroporated equal amounts of *Foxc>Msx* and *Foxc>NK4*, to see if the former could neutralize the latter's repressive effect on *Foxg* reporter expression and papilla formation. Indeed, co-electroporating *Foxc>Msx* and *Foxc>NK4* partially rescued *Foxg* reporter expression, resulting even in a large single protrusion in ~25% of cases (**Figure 7A-C**). This suggests that Msx can interfere with NK4 function, which may explain why the ventral papilla is able to form even in the presence of NK4. However, because the rescue was modest, there may be additional factors contributing to the de-repression of *Foxg* in the ventral papilla.

Chordin restricts NK4 expression and allows for dorsal papilla formation

Having found that Msx can interfere with NK4 function, which may explain how the ventral Foxg+ protrusion forms, we next sought to understand how the two dorsal protrusions are allowed to form. By *in situ* hybridization at the mid-tailbud stage, we could not rule out *NK4* expression from the dorsal papillae even though expression was weak and did not extend more dorsally (**Figure 5A,B**). We hypothesized that *NK4* might be downregulated at the very dorsal edges of the papilla territory, enough to allow for sustained *Foxg* expression in the cells that

239 eventually give rise to the two dorsal protrusions. Notably, the BMP antagonist Chordin is
240 expressed in the dorsal midline of the epidermis, immediately posterior to the dorsal papillae
241 (**Figure 7D, Figure S5**)(Imai et al., 2004; Liu et al., 2023). We hypothesized that Chordin might
242 be able to limit *NK4* expression more dorsally through its ability to antagonize BMP signaling.
243 Indeed, when we overexpressed Chordin (*Foxc>Chordin*), we obtained a similar effect as seen
244 with Noggin overexpression, in which a single papilla protrusion formed (**Figure 7E,F**). In
245 contrast, CRISPR/Cas9-mediated knockout of *Chordin* in the ectoderm significantly increased
246 *NK4* reporter plasmid expression in the papilla territory (**Figure 7G,H, Figure S6**). By
247 quantifying normalized mean *NK4>GFP* fluorescence, we demonstrated that its expression in
248 negative control larvae is indeed lower in the dorsal half of the papilla territory than in the ventral
249 (**Figure 7H, Figure S7**). CRISPR knockout of *Chordin* increased *NK4* reporter expression,
250 especially in the dorsal half of the papilla territory, closest to the source of Chordin (**Figure 7H**).
251 As expected, *Chordin* CRISPR suppressed dorsal *Foxg* reporter expression and dorsal papilla
252 formation (**Figure 7I,J**). Based on these data, we propose that Chordin limits the reach of BMP-
253 activated *NK4* expression on the dorsal side of the embryo, allowing for proper specification of
254 the dorsal papillae.
255
256
257 **DISCUSSION**
258
259 Here we present evidence for the involvement of NK4 as a key mediator of BMP signaling in
260 patterning the sensory-adhesive papillae of tunicate larvae. It was previously proposed that
261 BMP is required in the ventral papilla for the expression of an unknown, secreted factor that
262 activates the expression of Sp6/7/8 (also known as Zfp220), which in turn was proposed to
263 repress *Foxg* in interleaving cells to produce the tripartite organization of the papilla organ (Liu
264 et al., 2023; Liu and Satou, 2019; Roure et al., 2023). This was partially based on lack of clear
265 phosphoSMAD immunostaining outside the most ventral part of the papilla territory (Roure et
266 al., 2023). Here we show that the missing factor may be NK4, and that *Sp6/7/8* need not be
267 invoked. Instead of being secreted, NK4 is predicted to act cell-autonomously. We suggest that
268 NK4 expression is activated by low levels of BMP signaling, beyond the limits of robust
269 phosphoSMAD detection, which is consistent with our data and that of other studies tightly
270 linking *NK4* expression to BMP signaling (Christiaen et al., 2010; Roure et al., 2023; Waki et al.,
271 2015).
272

273 We propose that the patterning of the papillae can be explained by a classical morphogen
274 gradient (BMP) with *NK4* and *Msx* as targets, possibly at distinct activation thresholds (**Figure**
275 **8**). We show that NK4 is a transcriptional repressor that is necessary and sufficient to repress
276 *Foxg* in the papillae. A ventral-to-dorsal gradient of BMP signaling activates strong *NK4*
277 expression throughout much of the papilla territory but not at the dorsal-most extreme, where
278 we predict that BMP signaling is limited by dorsally-expressed Chordin. Here, *NK4* appears to
279 be downregulated by Chordin, allowing for *Foxg* expression to remain active, resulting in the left
280 and right dorsal papilla protrusions. In the ventral-most part of the papilla territory, where BMP
281 signaling is at its highest, we propose that Msx interferes with the ability of NK4 to repress *Foxg,*
282 contributing to the formation of the ventral papilla protrusion. Yet NK4 represses *Foxg* in all
283 other cells of the territory, and loss of BMP or NK4 results in ectopic *Foxg* activation throughout
284 and a single, large papilla (the "*Cyrano*" phenotype). Future work will be needed to confirm
285 some of these predictions, and to ascertain which regulatory connections are direct or indirect,
286 but this model is consistent with the data presented in the current study.
287
288 While our data strongly support a role for Chordin in antagonizing BMP and *NK4* expression in
289 the dorsal papillae it is still unclear if this activity extends to more ventral areas. In our *Chordin*
290 CRISPR larvae, different statistical tests were split on whether the increase in *NK4* reporter
291 expression was statistically significant in the ventral half of the papilla territory, compared to that
292 in negative control larvae (**Figure 7G,H**). Similarly, statistical tests were split on whether
293 knocking out *Chordin* results in more uniform *NK4* reporter expression along the dorsal-ventral
294 axis of the papillae. Accurate measurements may have been further hindered by the obvious
295 morphological defects in the dorsal papillae elicited by *Chordin* CRISPR (**Figure 7I,J**). Although
296 it is still not clear whether Chordin may affect the gradient of BMP signaling and *NK4* expression
297 across the entire papilla territory, our data suggests that the dorsal areas are more sensitive to
298 loss of Chordin function than the ventral areas. It is also unclear why *Foxg* is normally
299 downregulated at the very dorsolateral edges of the papilla territory, where presumably NK4
300 should not be present to repress it. Here, regulation of *Foxg* may be independent of BMP and
301 NK4, as suggested by the lower sensitivity of *Sp6/7/8* expression to BMP inhibition in these cells
302 as previously reported (Liu et al., 2023). Similarly, NK4 might not be needed to repress *Foxg* in
303 the very center of the papilla territory, which is derived from cells that never activate *Foxg* to
304 begin with (**Figure 1**)(Liu and Satou, 2019).
305

306 One outstanding question is how to reconcile this model with data supporting alternative
307 models. For instance, the MEK/ERK pathway (presumably downstream of FGF) was previously
308 suggested to limit *Islet* expression to the three spots/protrusions, with pharmacological inhibition
309 of MEK at the late neurula stage (stage 16) resulting in an expanded domain of *Islet* expression
310 similar to that seen with BMP inhibition or *NK4* CRISPR (Wagner et al., 2014). MEK inhibition
311 also suppresses the specification of Islet-negative cell types, such as outer collocytes and
312 papilla neurons (Johnson et al., 2024). It is possible that MEK/ERK signaling might provide a
313 temporal, not spatial, restriction on *Islet* expression. We know that MEK/ERK signaling is active
314 in the lineage at a slightly earlier stage to promote *Foxg* expression in papilla precursors (Liu
315 and Satou, 2019). If MEK/ERK signaling can repress *Islet* expression at this earlier stage (when
316 its upstream activator, Foxg, is already present), it would explain why *Islet* is normally not
317 expressed in a U-shaped territory like we see for *Foxg* early on. In other words, this might
318 constitute a time-delay mechanism to ensure that *Islet* is only expressed in three dots, after
319 *Foxg* expression has been refined. Future work would be needed to investigate this, with
320 carefully timed *in situ* hybridizations to see if *Islet* is indeed precociously activated upon MEK
321 inhibition. Another unresolved question is the exact role(s) of Sp6/7/8 in patterning the papillae.
322 Previously we have shown that Sp6/7/8 is required for the proper specification of collocytes in
323 the papillae, but this appears to complement, not repress, Foxg-mediated gene expression
324 (Johnson et al., 2024). Furthermore, Sp6/7/8 is expressed in papilla neuron progenitors, but is
325 not required for neurogenesis (Johnson et al., 2024). Neither BMP inhibition nor *NK4* CRISPR
326 appear to prevent the formation of collocytes or papilla neurons, suggesting that more work will
327 be needed to study the precise regulatory relationship between Sp6/7/8 and Foxg.
328
329 Finally, our model relies on some kind of interference with NK4 function by Msx. How might this
330 work, molecularly speaking? Both Msx and NK4 belong to the NKL subclass of homeobox
331 transcription factors (Holland et al., 2007). NK4 orthologs have been shown to dimerize
332 (Kasahara et al., 2000; Zaffran and Frasch, 2005), and the residues in the homeodomain
333 required for dimerization (Kasahara et al., 2001) appear to be shared between *Ciona* NK4 and
334 Msx (**Figure S8**). One possibility is that co-expression of Msx and NK4 forces the formation of
335 Msx:NK4 heterodimers that are unable to repress *Foxg.* Alternatively, Msx simply competes for
336 NK4 binding sites in the *Foxg* promoter. Future work will elucidate the molecular basis for the
337 ability of Msx to relieve NK4-mediated repression. In our experiments, Msx co-expression only
338 partially alleviated the repressive effect of NK4, suggesting there may be additional factors

339 expressed in the ventral medial papilla working together with Msx to promote *Foxg* activation
340 there.
341
342
343
344 **MATERIALS AND METHODS**
345
346 **Ciona handling and electroporation**
347 Gravid adult specimens of *Ciona robusta* (*intestinalis* Type A) were collected and shipped by
348 Marinus Scientific (Lakewood, CA) or M-REP (Carlsbad, CA). Gametes were isolated from
349 adults and fertilized *in vitro* and dechorionated as previously described (Christiaen et al.,
350 2009b). Electroporation of dechorionated, synchronized zygotes was carried out as previously
351 described (Christiaen et al., 2009a). Plasmid DNA electroporation amounts were calculated and
352 listed as total micrograms per 100 µl, for a final electroporation volume of 700 µl (including D-
353 mannitol solution and sea water). DNA sequences and amounts are listed in the **Supplemental**
354 **Sequences** file. Embryos, larvae, and juveniles were reared at 20°C, and staged according to
355 hours post-fertilization (hpf) and Hotta Staging (Hotta et al., 2020). To monitor metamorphosis,
356 larvae were transferred at 17 hpf (Hotta Stage 27) to a new agarose-coated 10 cm petri dish
357 with 400 µl of 100X penicillin-streptomycin stock solution (Gibco) added to each dish. Juveniles
358 were collected at 44 hpf (stage ~35) and fixed according to the same protocol as for larvae.
359 Larvae were collected and fixed at 17 hpf, unless otherwise noted.
360
361 **Immunofluorescence, *in situ* hybridization, and imaging**
362 Larvae and embryos were fixed as previously described for whole-mount mRNA *in situ*
363 hybridizations (Stolfi and Levine, 2011) or for immunofluorescence or fluorescent protein
364 imaging (Vedurupaka et al., 2025). *In situ* hybridizations were carried out as previously
365 described (Stolfi and Levine, 2011). *Foxg* and *NK4* probes were previously published (Johnson
366 et al., 2020). Acetylated tubulin antibody staining was performed modified from a published
367 protocol (Pennati et al., 2015). Briefly, larvae were fixed by direct addition of 16%
368 paraformaldehyde (250 µl for a 10 cm dish), then washed four times in PBS + 0.1% Tween-20.
369 Larvae were incubated at 4°C overnight in mouse anti-acetylated primary antibody (Sigma-
370 Aldrich catalog# MABT868) diluted 1:200 in PBS + 1% BSA, then washed four times in PBT.
371 Secondary antibody (donkey anti-mouse AlexaFluor-488, ThemoFisher catalog# A21202) was
372 incubated at 1:400 in PBS + 1% BSA again overnight at 4°C. Final washes were performed as

373 before, prior to incubating with DAPI and mounting. Images were acquired on Leica DMIL LED
374 or DMI8 inverted compound epifluorescence microscopes, or a Zeiss LSM 900 laser-scanning
375 confocal microscope. Images acquired on Leica microscopes were processed and exported
376 using LASX software, while confocal images were processed using the ZEN software suite. For
377 scoring, only embryos/larvae expressing *Foxc>H2B::mCherry* in the papillae were scored,
378 unless otherwise specifically noted.
379
380 **NK4 reporter fluorescence quantification and normalization**
381 Fixed, slide-mounted larvae were imaged on a Leica DMI8 inverted compound epifluorescence
382 microscope using the same illumination and exposure settings between larvae (though settings
383 changed depending on whether it was GFP or mCherry fluorescence being imaged. For the
384 Noggin overexpression experiment, the 20X objective (HC PL FLUOTAR L, 0.40 N.A., 0-2 mm
385 correction collar) was used to image both the papillae and most of the larva (excluding the tail
386 tip). For the Chordin CRISPR experiment, the 40X objective (HC PL APO, 0.95 N.A., 0.11-0.23
387 mm correction collar) was used to image mostly the head including the papillae. After image
388 acquisition, regions of interest (ROIs) were drawn in Leica LASX software, and mean
389 fluorescence pixel intensity values exported for further analysis and plotting. For the Noggin
390 overexpression experiment, an ROI around the papilla region and another ROI around the
391 whole larva was drawn for each individual. For the Chordin CRISPR experiment, one ROI was
392 drawn around the ventral half of the papilla region, and another around the dorsal half of the
393 papilla region, for each individual. Raw pixel intensity measurements and calculated
394 GFP/mCherry ratios can be found in **Supplemental Data S1**.
395
396 **Tissue-specific CRISPR/Cas9-mediated mutagenesis in F0**
397 CRISPR/Cas9-mediated mutagenesis in electroporated embryos was carried out as previously
398 described (Popsuj et al., 2024). The original *NK4*-targeting sgRNA (*NK4.3*) was previously
399 published and validated by in-house Illumina amplicon sequencing (Gandhi et al., 2017). A
400 negative control ("Control") sgRNA targeting no *Ciona* sequence was previously published
401 (Stolfi et al., 2014). An additional sgRNA (*Defcab.*47) targeting the *Defcab* gene (Gibboney et
402 al., 2020; Kim et al., 2025), which is not expressed in the papillae, was similarly used as a
403 negative control in one experiment (**Figure 5D-E**). New sgRNAs targeting *NK4* and *Chordin*
404 were designed using CRISPOR (Concordet and Haeussler, 2018; Haeussler et al., 2016), and
405 validated by Amplicon E-Z sequencing service by Genewiz/Azenta (South Plainfield, NJ) as
406 previously described (Johnson et al., 2023; Popsuj et al., 2024). The validation protocol can also

be followed at dx.doi.org/10.17504/protocols.io.14egnr97yl5d/v1 (Popsuj et al., 2024). Cas9 was frequently fused to Geminin$^{N\text{-terminus}}$, which increases mutagenesis efficacy (Pennati et al., 2024; Song et al., 2022). All sgRNA, Cas9, primer, and relevant plasmid DNA sequences and amounts are included in the **Supplemental Sequences** file.

ACKNOWLEDGMENTS

The authors would like to thank Dr. Florian Razy-Krajka for cloning parts of the *Chordin* promoter and coding sequences, and Dr. Robbie Richards for advice on statistical analyses. The authors also thank Dr. Eduardo Gigante and Hussan Ali for cloning and characterizing the *Noggin* coding sequence. The authors are grateful to other past and present members of the Stolfi and Cota labs for feedback and suggestions. This work was funded by NIH grants R35GM158421 to AS and R01HD104825 to CDC and AS, NSF (IOS) grant 2052493 to CDC, and an NSF Graduate Fellowship to CJJ. The authors declare no conflicts of interest.

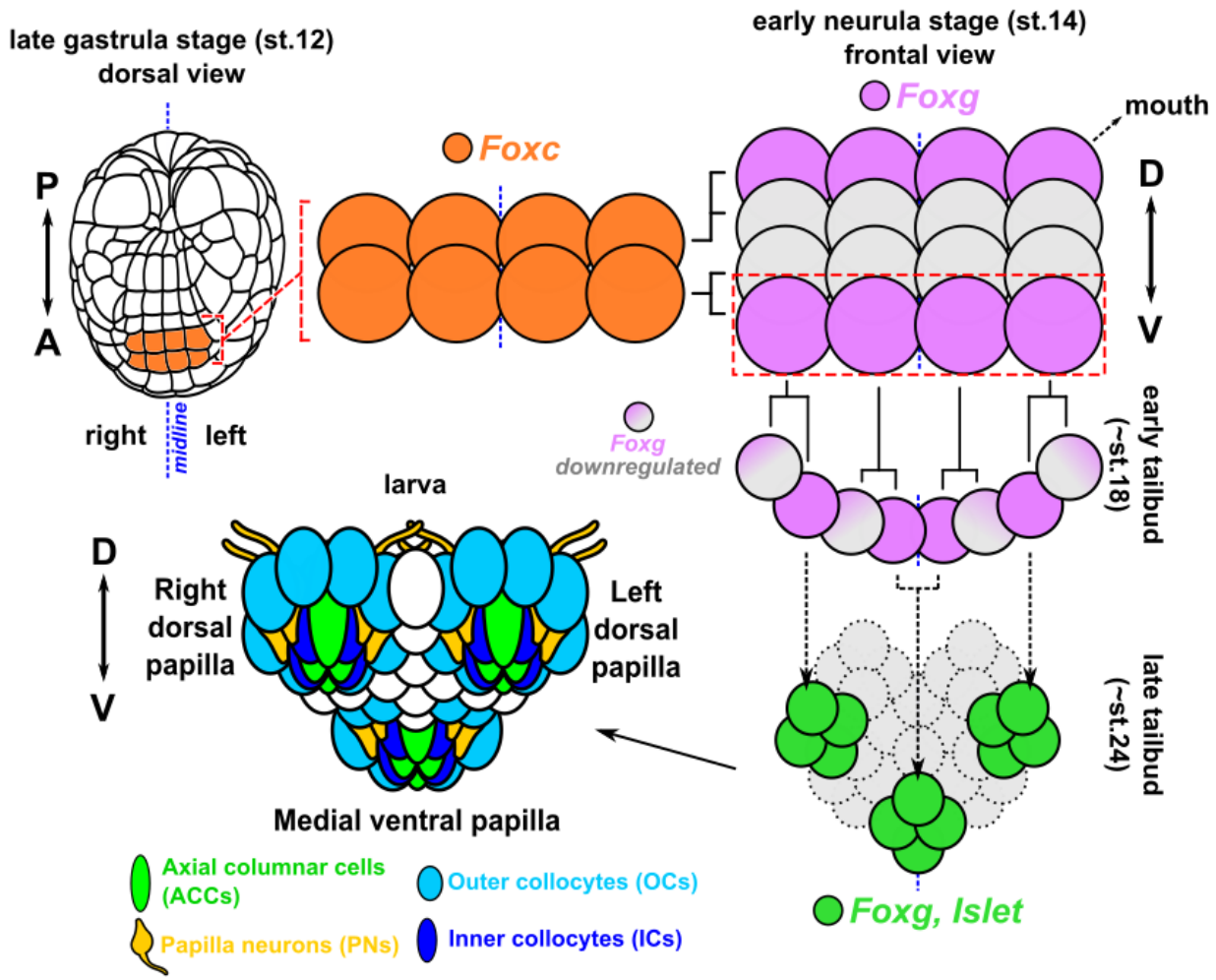

Figure 1. Summary diagram of papilla development in *Ciona.*

A stylized diagram summarizing what is currently know about the cell lineages and major cell fate specification events in the developing papilla territory of *Ciona* embryos. Briefly, the papillae are derived from anterior-most *Foxc*-expressing cells of the anterior neural plate border at gastrula stage. The anterior-most row of daughter cells (red dashed rectangle) go on to express *Foxg* at the early neurula stage. During tailbud stages, this row of cells begins to bend ventrally, forming a “U”-shaped swatch of cells. *Foxg* expression is maintained in three discrete clusters of cells and downregulated in the remaining cells of this row. Eventually, sustained Foxg activates *Islet* in the three cell clusters and their descendants, giving rise to the three protruding sensory-adhesive papillae of the hatched larva: one medial, one ventral papilla, and two lateral, dorsal papillae. Each papilla is composed of invariant numbers of different cell types (4 axial columnar cells, 4 inner collocytes, 4 papilla neurons, and 8 outer collocytes, for a total of 20 cells). See text for references.

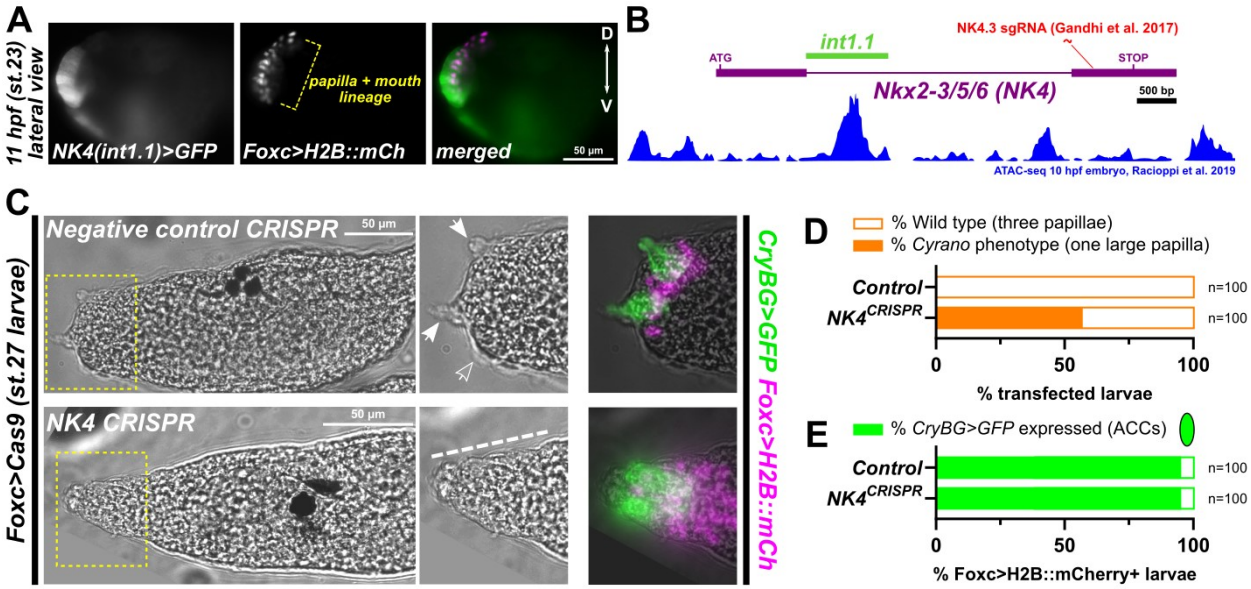

Figure 2. *NK4,* an *NKX2-3/5/6* ortholog, is required for the tripartite patterning of the papillae.

A) A GFP reporter plasmid constructed using a portion of the sole intron of the *NK4* gene of *Ciona robusta* ("int1.1"), fused to the basal promoter of the *FOG* gene (Rothbächer et al., 2007). See **Supplemental Sequences** file for details), is expressed throughout the Foxc+ papilla territory in stage 23 embryos, recapitulating the previously reported mRNA *in situ* hybridization pattern. Int1.1 reporter activity can also be seen in ventral epidermis and trunk endoderm. hpf = hours post-fertilization. B) Diagram depicting the *NK4* locus and location of both the int1.1 *cis*-regulatory element and the target of the published *NK4.3* sgRNA. Underneath is the ATAC-seq profile of 10 hpf embryos, from Racioppi et al. 2019, showing a peak of DNA accessibility centered on the int1.1 element. C) Papilla lineage-specific CRISPR/Cas9-mediated mutagenesis of *NK4* showing the single, enlarged papilla protrusion (indicated by dashed line) similar to the *Cyrano* phenotype described in Roure et al. 2023 and replicated in Liu et al. 2023. Compare to the negative control CRISPR using the non-targeting *"Control"* sgRNA instead. Right panels: the *CryBG>GFP* reporter (green) reveals the presence of ACCs in the single papilla of the *NK4* CRISPR larvae. Left panels show brightfield images (zoomed in panel indicated in yellow dashed outline), while right panels show brightfield overlaid on GFP/mCherry fluorescence. D) Scoring the percentage of transfected larvae showing the single large papilla phenotype ("*Cyrano*") in *NK4* CRISPR vs. negative control larvae electroporated with only the reporter plasmids. Transfection was monitored using a combination of *Islet>GFP* and *Foxc>H2B::mCherry* reporter plasmid expression in the papillae. E) Scoring the proportion of transfected (*Foxc>H2B::mCherry+*) larvae showing *CryBG>GFP* expression as shown in panel

C. No difference was observed in the proportion of larvae expressing *CryBG>GFP* between *NK4* CRISPR and control larvae. All GFP sequences are tagged with Unc-76, which promotes cytoplasmic localization over nuclear localization (Dynes and Ngai, 1998). Scale bars = 50 m. mCh: mCherry; D: dorsal; V: ventral.

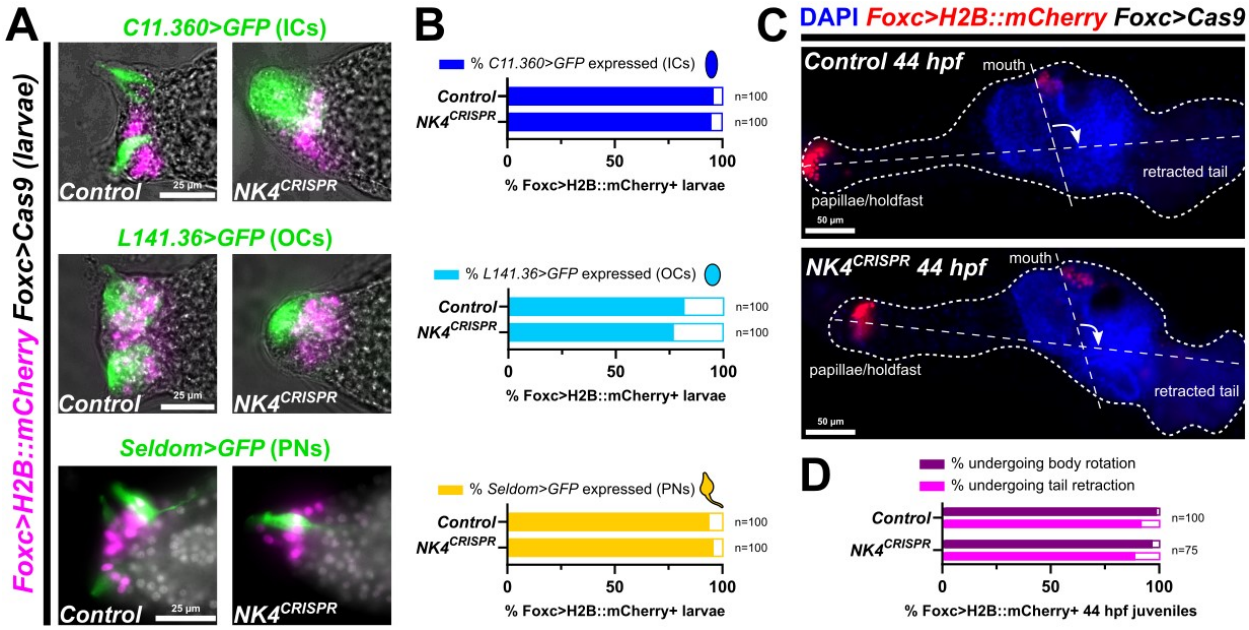

Figure 3. *NK4* CRISPR does not significantly impact specification of other papilla cell types or metamorphosis, despite resulting in a single large papilla.

A) Papilla lineage-specific *CRISPR* mutagenesis of *NK4* does not result in loss of other papilla cell type-specific reporter gene expression in spite of the loss of the typical tripartite organization of the papillae. ICs: inner collocytes; OCs: outer collocytes; PNs: papilla neurons. Counterstain in *Seldom>GFP* images is DAPI (white overlay). Scale bars = 25 µm. IC and PN images acquired at 17 hours post-fertilization (hpf; St. 27), while OC images were acquired at 21 hpf (St. 29) on account of the late onset of *L141.36* expression as previously reported (Johnson et al., 2024). B) Scoring the percentage of transfected larvae showing expression of each cell type-specific reporter, comparing *NK4* CRISPR vs. negative control larvae as indicated in panel A. C) *NK4* CRISPR in the papilla lineage also does not significantly prevent metamorphosis, as assayed in 44 hpf juveniles (St. 35) undergoing tail retraction and body axis rotation (white arrow). Scale bars = 50 µm. D) Scoring the percentage of transfected juveniles undergoing either metamorphic process as depicted in panel C. All GFP sequences tagged with Unc-76.

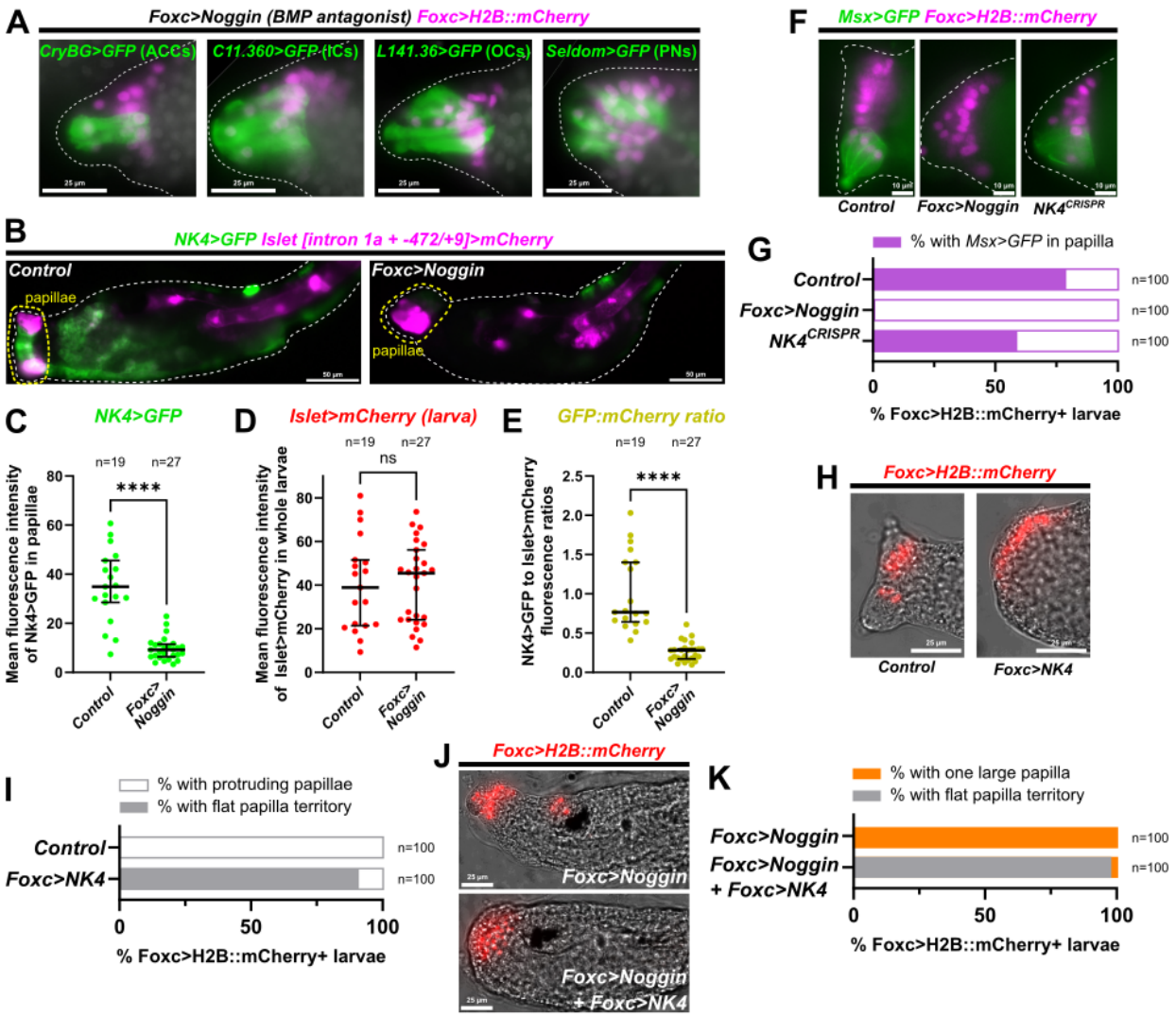

Figure 4. NK4 acts downstream of BMP signaling in the papillae.

A) Overexpression of the BMP antagonist Noggin in the papilla lineage (using *Foxc>Noggin* plasmid) results in a "*Cyrano"* phenotype similar to *NK4* CRISPR: a single large papilla containing all four papilla cell types (ACCs, ICs, OCs, adn PNs). DAPI counterstain shown in white overlay. All at 17 hpf (St. 27) except *L141.36* reporter expression, which is visible only around 21 hpf (St. 29). B) *NK4*>GFP reporter expression (green) was quantified by measuring mean fluorescence in the papilla territory (yellow dashed area), in negative control and *Foxc>Noggin*-electroporated larvae. Transfection efficacy was normalized using whole-larva expression of *Islet [intron 1a + -472/+9]>mCherry* (magenta), which is expressed in papilla and notochord cells. Scale bars = 50 µm. C) Comparison of mean fluorescence intensity readouts of *NK4>GFP* expression in the papilla region (as indicated in panel B), between negative control and *Foxc>Noggin* larvae. Data show significant downregulation of *NK4* reporter expression in the papillae by Noggin overexpression. 5 outliers of fluorescence over 80 were removed from

548 the control dataset. **** p<0.0001 by two-tailed Mann-Whitney test. D) Comparison of mean
549 fluorescence intensity readouts of *Islet>mCherry* fluorescence in the whole larva, between the
550 same larvae plotted in panel C and shown in panel B. Data show that overexpression of Noggin
551 had no significant effect on Islet expression levels throughout the larva, indicating comparable
552 transfection efficacies and suitable use of whole-larva *Islet* reporter expression to normalize
553 *NK4* reporter activity. p = 0.7404 by two-tailed Mann-Whitney. E) Ratio of GFP to mCherry
554 intensity values plotted in panels C and D, showing that *NK4* reporter is significantly
555 downregulated by Noggin overexpression even when normalized by transfection efficacy.
556 p<0.0001 by two-tailed Mann-Whitney. Outliers with GFP:mCherry ratio >3.0 (three in the
557 control condition) were removed from the entire dataset. Complete data with flagged outliers
558 can be found in **Supplemental Data S1.** Normalization to papilla-specific *Islet>mCherry*
559 expression can be found in **Figure S3.** F) Expression of the *Msx>CD4::GFP* reporter (green) in
560 negative control CRISPR, Noggin overexpression, and *NK4* CRISPR (using *Foxc>Cas9*). G)
561 Comparison of percentage of transfected larvae showing *Msx* reporter expression in the ventral
562 papilla region, comparing the conditions shown in panel F. H) Overexpression of NK4 using the
563 *Foxc* promoter results in the absence of protruding papillae and flattening of the entire anterior
564 epidermis. I) Scoring the percentage of transfected larvae showing the flattened papilla territory,
565 comparing the conditions in panel H. J) Overexpression of NK4 in the papilla region can
566 override the Noggin overexpression phenotype, converting a single large papilla into a flattened
567 epidermis. All scale bars (except in panel B) = 25 μm. All GFP sequences except
568 *Msx>CD4::GFP* are tagged with Unc-76.
569
570
571
572
573
574
575
576
577
578
579
580
581

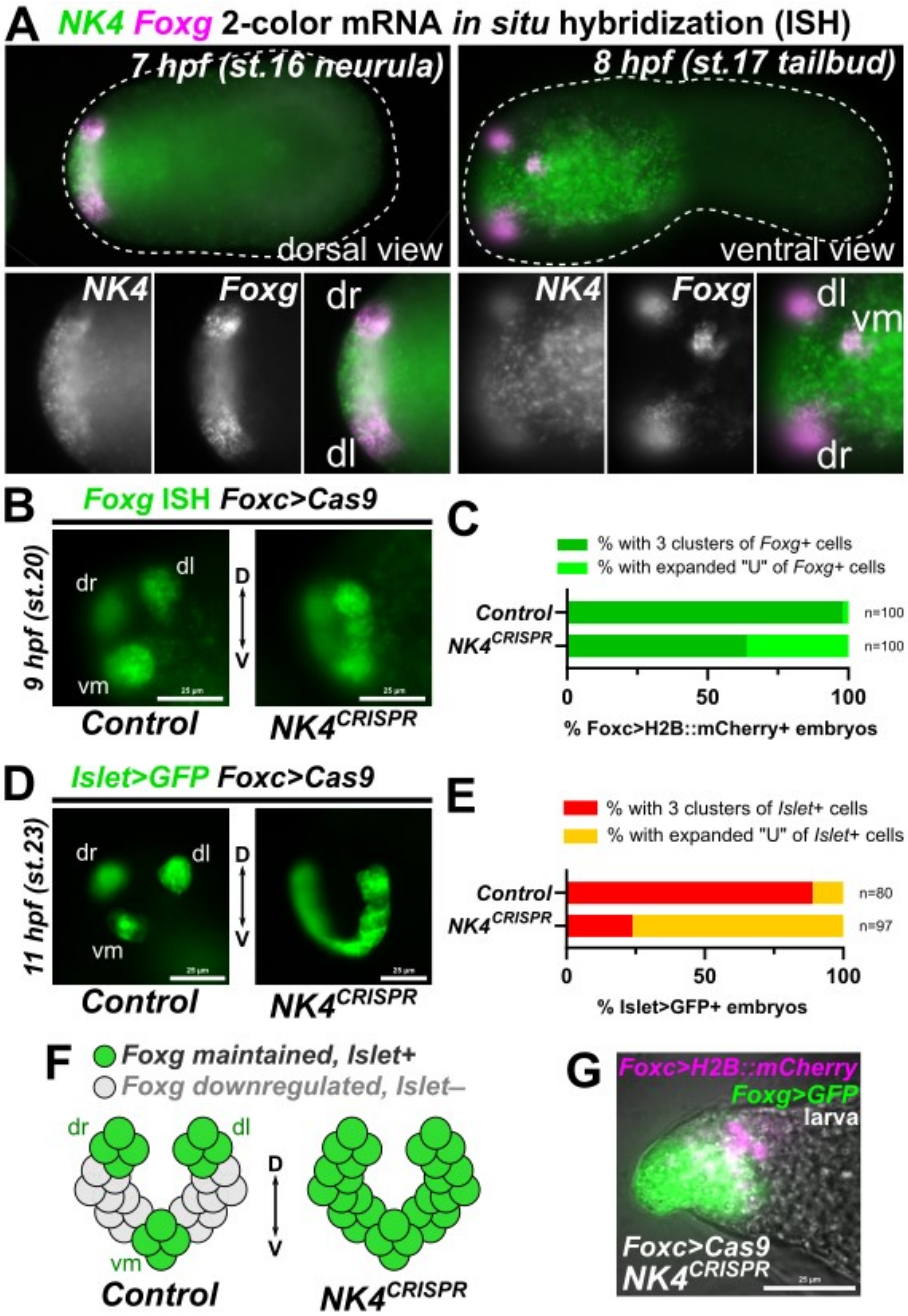

Figure 5. *NK4* CRISPR expands *Foxg* and *Islet* expression.

A) Whole-mount, two-color fluorescent mRNA *in situ* hybridization showing *Foxg* (green) and *NK4* (magenta) expression in the papilla territory. Left: dorsal view at neurula stage, showing that *NK4* expression does not extend dorsally or laterally beyond the dorsal limits of *Foxg* expression. Right: ventral view at tailbud stage, showing strong *NK4* expression in ventral areas including the ventral *Foxg+* cells that will give rise to the ventral medial papilla. hpf = hours post-fertilization. This is a different focal plane of the same embryo imaged for a previous publication (Johnson et al. 2020). B) *In situ* hybridization of *Foxg* at 9 hpf (mid tailbud), showing expansion

591 from three spots to a “U” shape swath of cells upon *NK4* CRISPR, compared to negative control
592 CRISPR embryos. C) Scoring percentage of transfected embryos showing expanded *Foxg*
593 expression as shown in panel B. D) Expansion of *Islet>GFP* reporter expression at 11 hpf (late
594 tailbud) upon *NK4* CRISPR. Control embryos were instead electroporated with the *Defcab.47*
595 sgRNA, targeting a gene that is not expressed in the papillae (see **materials and methods** for
596 details). E) Scoring of transfected embryos showing expanded *Islet* reporter expression as seen
597 in panel D. F) Summary diagram explaining our interpretation of expanded *Foxg* and *Islet*
598 expression in *NK4* CRISPR embryos. G) *NK4* CRISPR larva showing *Foxg* reporter expression
599 (green) in the resulting single large papilla. dr: dorsal right; dl: dorsal left; vm: ventral medial; D:
600 dorsal; V: ventral. All scale bars = 25 μm. All GFP sequences are tagged with Unc-76.
601
602
603
604
605
606
607
608
609
610
611
612
613
614
615
616
617
618
619
620
621
622
623
624

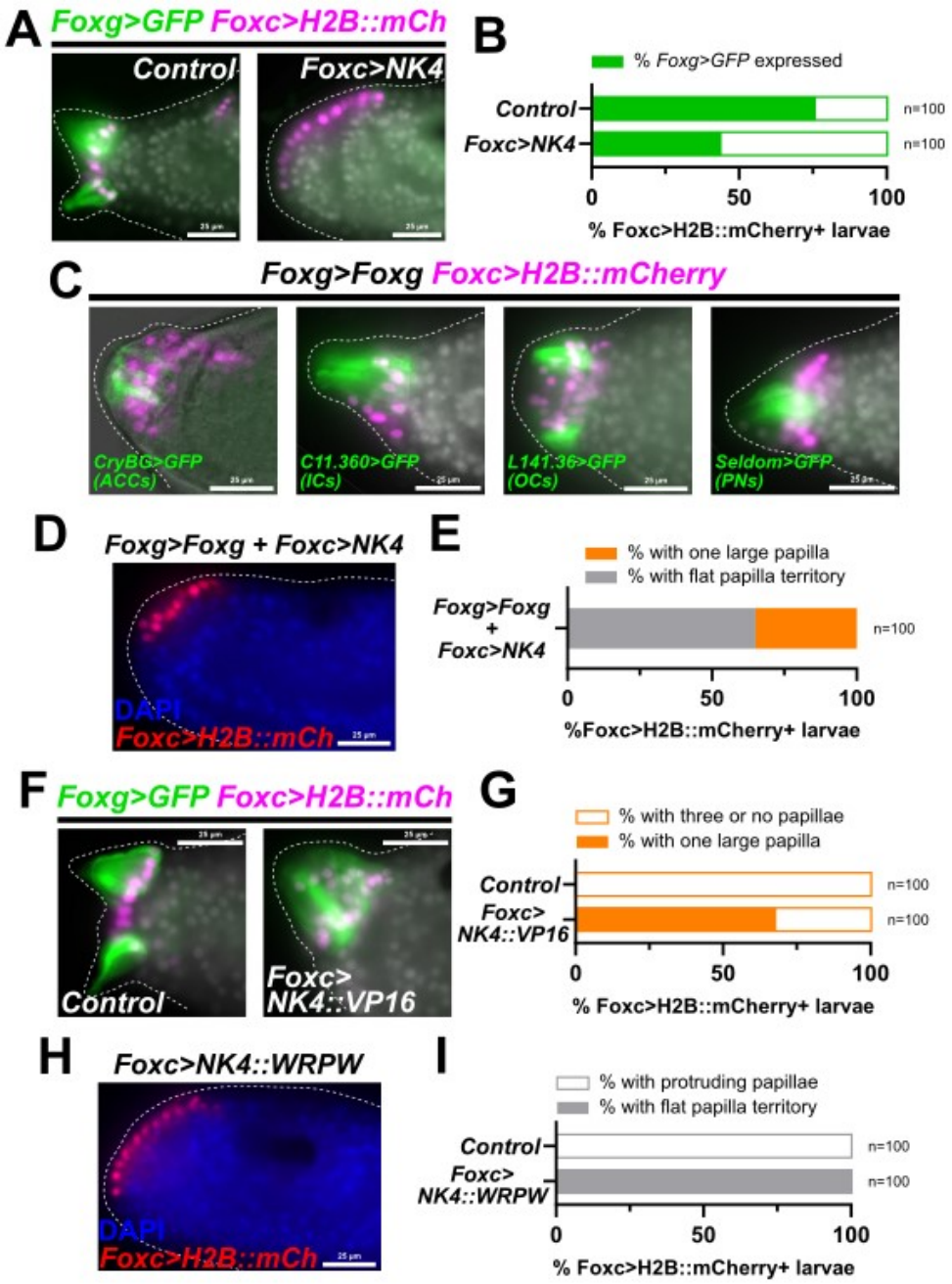

Figure 6. NK4 acts as a transcriptional repressor to suppress *Foxg* expression in the papillae.

A) Overexpression of NK4 suppresses *Foxg* reporter expression (green) in the flattened papilla region. B) Scoring of larvae showing *Foxg* reporter expression, showing reduction upon NK4 overexpression compared to negative control larvae. C) Overexpression of *Foxg* by electroporating the *Foxg>Foxg* plasmid results in a single large papilla containing all four cell types, similar to that seen in *NK4* CRISPR and Noggin overexpression. OCs imaged at 21 hpf (St. 29) due to later onset of *L141.36* expression. ACC experiment conducted in a *Foxg*

634 CRISPR background and imaged at 19 hpf (St. 28) as part of a rescue experiment described
635 previously (Johnson et al., 2024), see **Supplemental Sequences** file for details. D) Single large
636 papilla elicited by Foxg overexpression can be suppressed by co-overexpression of NK4. E)
637 Scoring the percentage of transfected larvae showing either a single large papilla or a flat
638 papilla territory upon overexpression of Foxg and NK4 combined. F) The C-terminus of NK4 (C-
639 terminal to the homeodomain) was replaced with a VP16 transactivation domain.
640 Overexpression of this NK4::VP16 construct resulted in a single large papilla with robust
641 *Foxg>GFP* expression. G) Scoring the percentage of transfected larvae showing a single large
642 papilla, comparing NK4::VP16-ovexpressing larvae to negative control larvae. NK4::VP16 also
643 resulted in 30% larvae with no protruding papillae. H) Overexpression of NK4::WRPW, in which
644 the C-terminus of NK4 is replaced with the WRPW Groucho co-repressor recruitment domain.
645 This phenocopied full-length NK4 overexpression, suggesting NK4 normally acts as a
646 transcriptional repressor in the papilla territory. I) Scoring the percentage of transfected larvae
647 with either normal, protruding papillae or flat/no papillae, comparing NK4::WRPW
648 overexpression to negative control larvae. All counterstained with DAPI (white or blue overlay)
649 except *CryBG/*ACC image in panel C. All GFP sequences fused to Unc-76. All scale bars = 25
650 µm. mCh: mCherry.
651
652
653
654
655
656
657
658

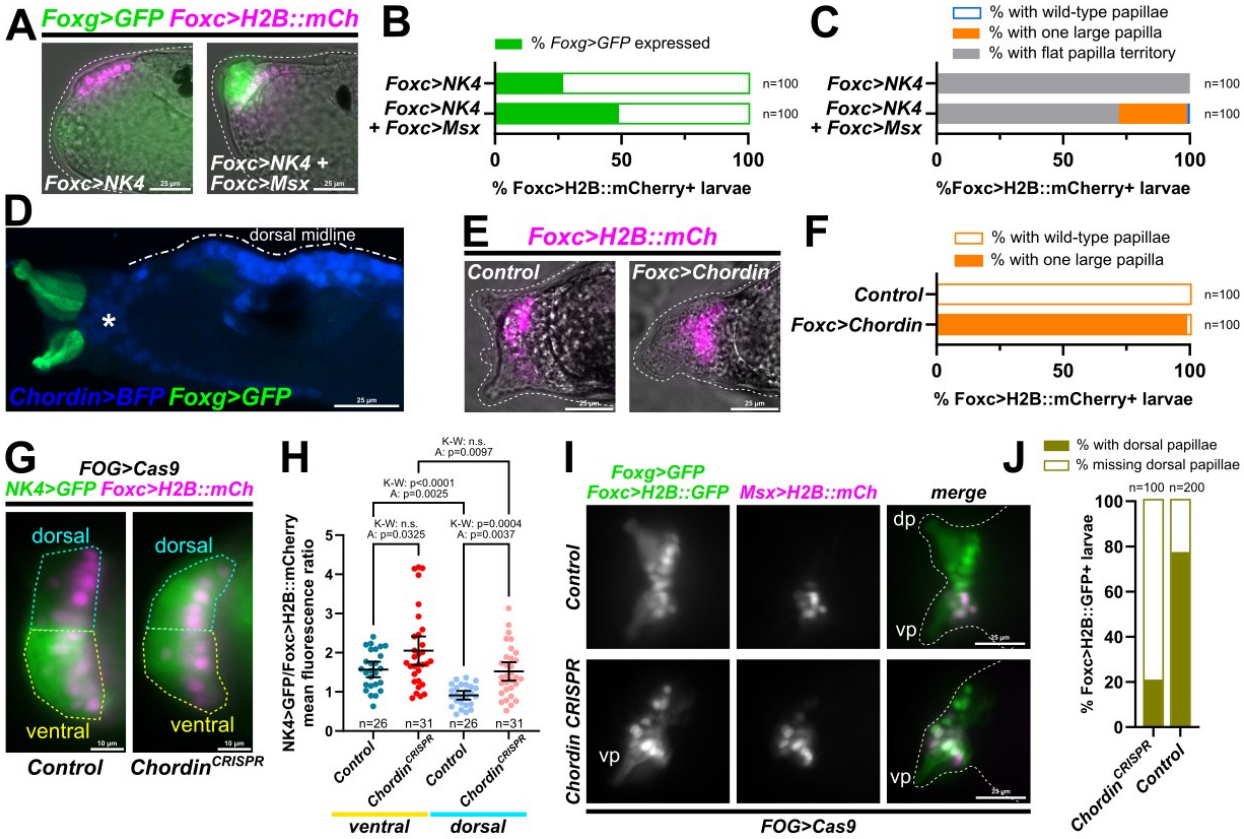

Figure 7. Regulation of NK4 expression and activity by Msx and Chordin.

A) Overexpression of the ventral papilla-specific regulator Msx can partially rescue the NK4 overexpression-induced loss of *Foxg* reporter expression and papilla formation B) Scoring the percentage of transfected larvae showing *Foxg>GFP* reporter expression, comparing NK4 and Msx co-overexpression vs. NK4 overexpression alone, as shown in panel A. C) Scoring the percentage of larvae showing a flat papilla territory, a single large papilla, or the normal three papillae, comparing the conditions in panels A and B. D) a larva co-electroporated with *Chordin>TagBFP* (blue) and *Foxg>GFP* (green) reporter plasmids. *Chordin* is expressed in dorsal midline cells just posterior to the dorsal papillae (Liu et al., 2023). Asterisk denotes migratory mesenchyme cells, which also express *Chordin* at the tailbud stage (Imai et al., 2004). E) Overexpression of Chordin in the papilla territory phenocopies Noggin overexpression, suggesting it antagonizes BMP signaling as predicted. F) Scoring the percentage of transfected larvae showing either wild-type three normal papillae or a single large papilla, comparing Chordin overexpression and negative control larvae, as in panel E. G) Examples of the papilla territory divided into ventral and dorsal halves and imaged for *NK4>GFP* (green) and *Foxc>H2B::mCherry* (magenta) quantification, divided into dorsal and ventral halves, to compare *NK4>GFP* expression in negative control and *Chordin* CRISPR larvae. Scale bars =

677 10 μm. H) Ratios of GFP to mCherry mean fluorescence intensities were calculated for ventral
678 and dorsal halves, across control and *Chordin* CRISPR conditions as shown in panel G. One-
679 way ANOVA and Kruskal-Wallis tests were performed in parallel as the data for ventral papillae
680 in *Chordin* CRISPR was not normally distributed on account of a few outliers. See text for
681 discussion of possible interpretations. n.s.: not significant ($p>0.05$). I) *Chordin* CRISPR can
682 eliminate the dorsal papillae, which are labeled by *Foxg>GFP* (green cytoplasm) but are
683 negative for *Msx>H2B::mCherry* (magenta). dp: dorsal papilla(e), vp: ventral papilla. Scoring of
684 larvae expressing *Foxc>H2B::GFP+* (green nuclei), showing presence or absence of dorsal
685 papillae in control or *Chordin* CRISPR conditions as seen in panel I. All GFP sequences fused
686 to Unc-76 except otherwise noted. All scale bars = 25 μm unless otherwise specified.
687
688
689
690
691
692
693
694
695
696
697
698
699
700
701
702
703
704
705
706
707
708
709

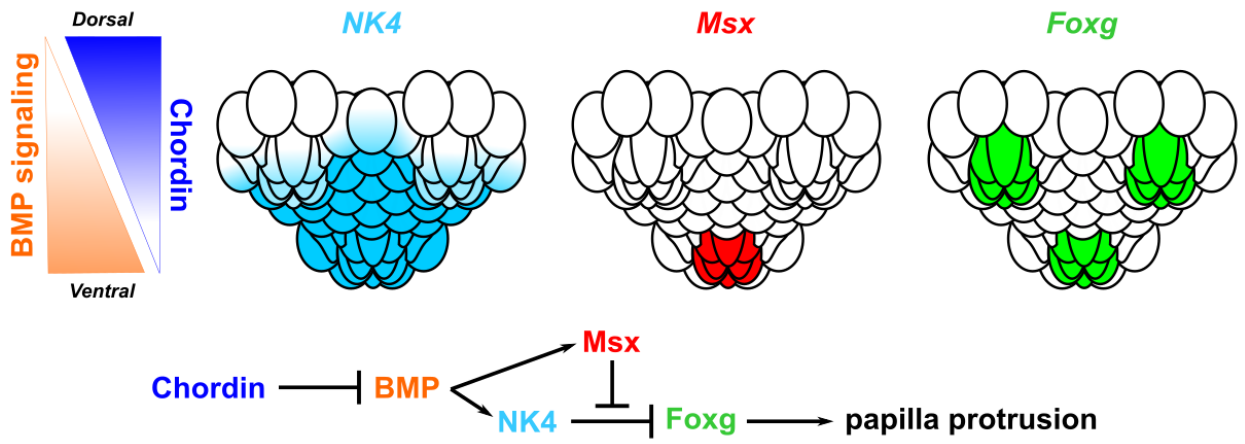

Figure 8. The proposed role of NK4 downstream of BMP in the papillae.
A diagram summarizing the main points of the current work. Top left: A ventral-to-dorsal gradient of BMP signaling is shaped in part by an opposing, dorsal-to-ventral gradient of the BMP antagonist Chordin. Top right: expression domains of *NK4, Msx,* and *Foxg* in the papilla territory (dorsal at top). According to our proposed model, NK4 downregulates *Foxg* in certain intervening cells, but Msx may interfere with NK4 function in the ventral-most cells. Bottom: proposed regulatory network in which NK4 downregulates *Foxg* downstream of BMP signaling.

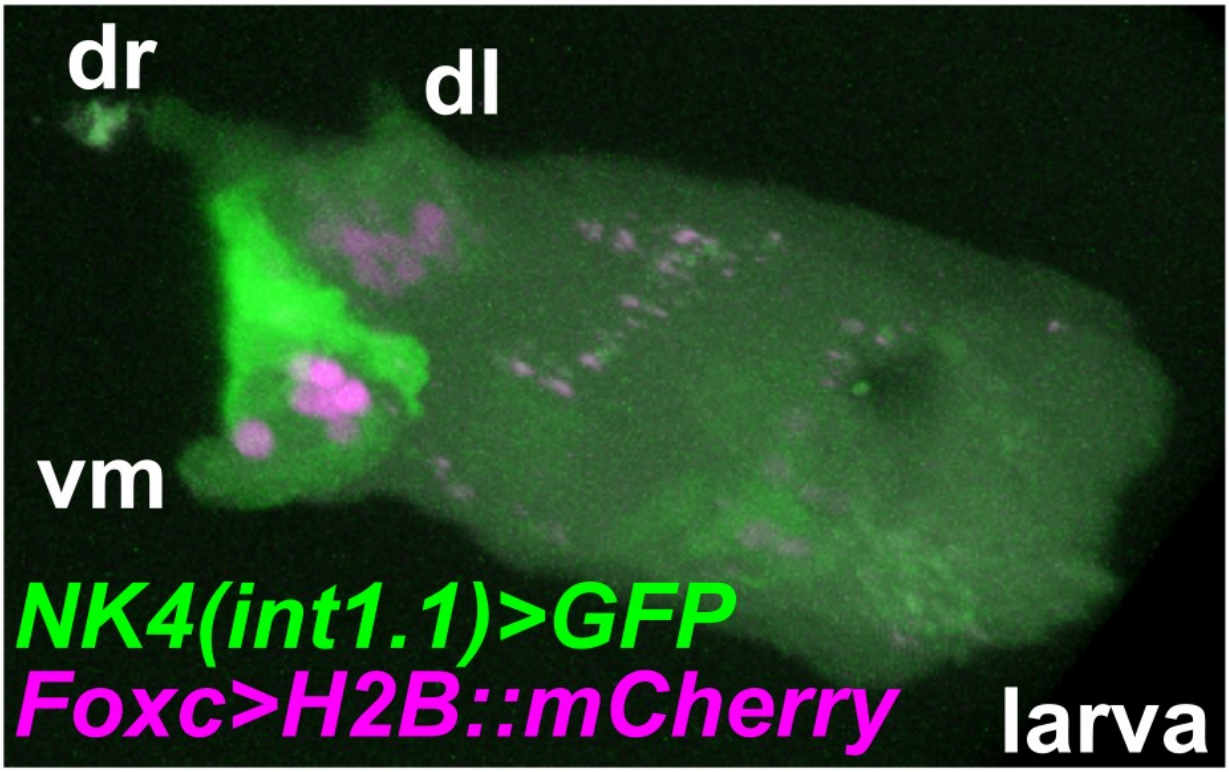

Supplemental Figure S1.

3D confocal projection of the head of a larva showing the *NK4* and *Foxc* reporters labeling the papilla territory. Note strong *NK4(int1.1)+bpFOG>Unc-76::GFP* expression (green) in cells located in between the three papillae, as well as in the ventral medial (vm) papilla, though it appears weak if not absent from the dorsal right (dr) and dorsal left (dl) papillae.

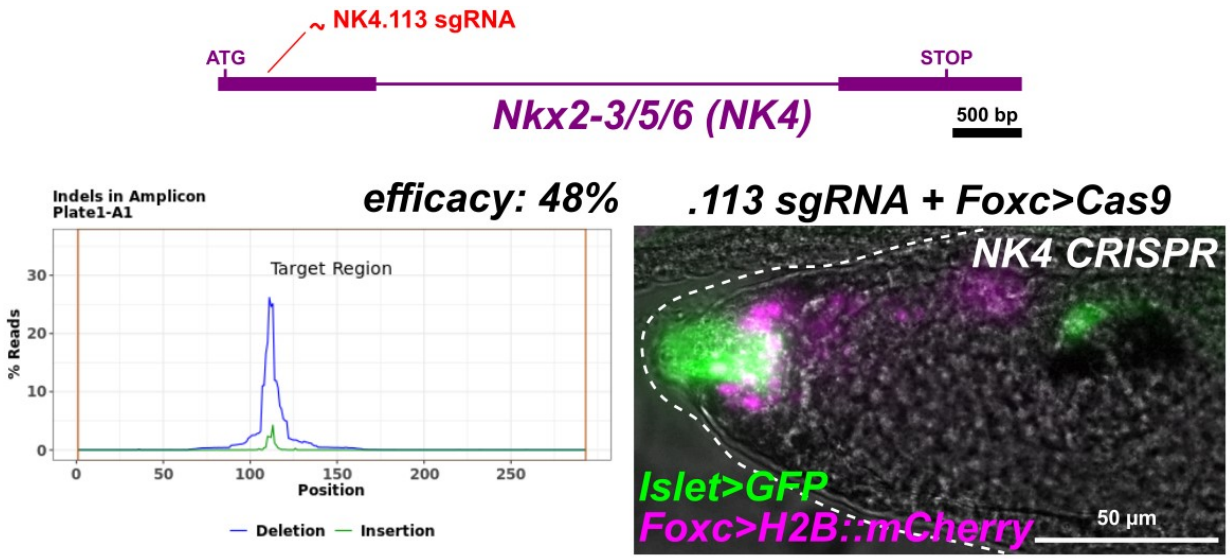

Figure S2.

A second sgRNA (NK4.113) newly designed to target the first exon of *NK4* also results in a single large papilla. *Islet>GFP = Islet intron 1a + -473/+9>Unc-76::GFP.* The efficacy as measured by Illumina amplicon sequencing was 48%.

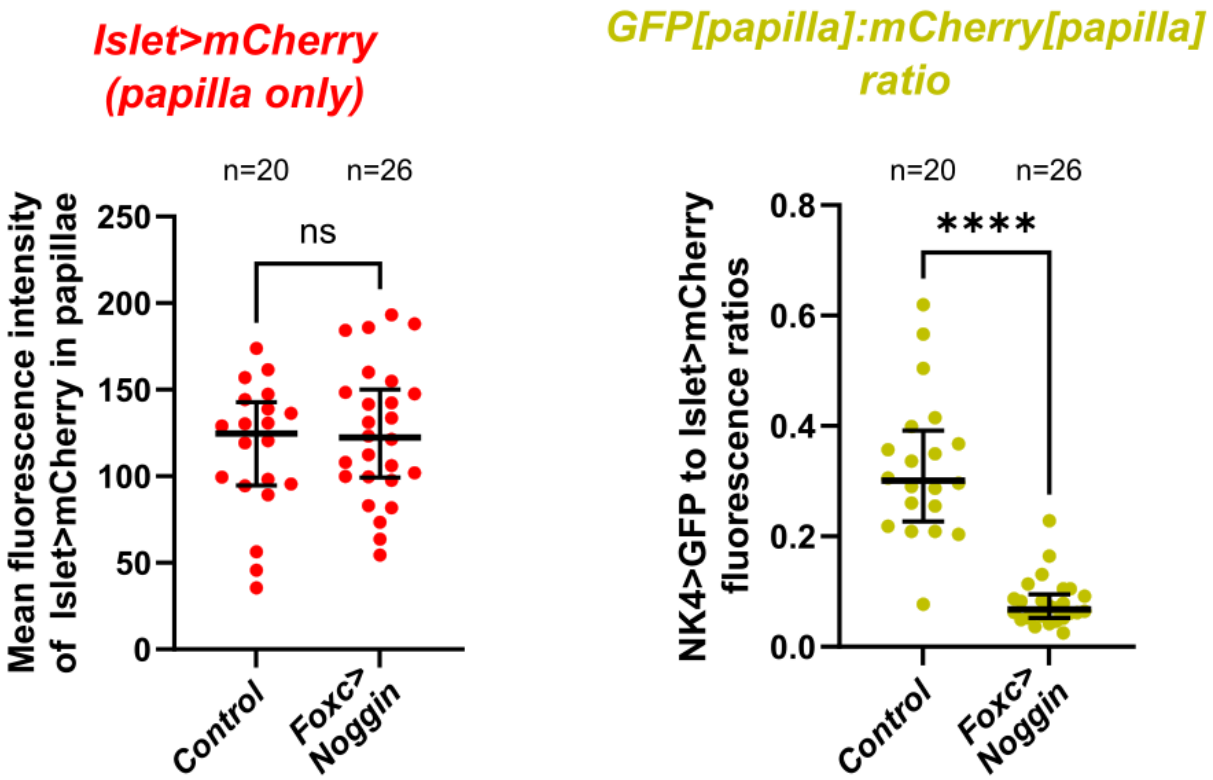

Figure S3.

Comparison of mean fluorescence intensity readouts of *Islet>mCherry* fluorescence in the papilla territory only (unlike in main Figure 4D, which shows quantification of mean fluorescence intensity of *Islet>mCherry* in the whole larva), between negative control and *Foxc>Noggin* conditions as shown in Figure 4. Left: data show no significant effect on Noggin on Islet expression levels in the papilla, similar to how there was no significant effect on Islet expression throughout the larva. p = 0.6613 by two-tailed unpaired t-test. Right: ratio of *NK4>GFP* and *Islet>mCherry* mean fluorescence values in the papillae (unlike in the main figure 4E, which showed the ratio between GFP in the papillae and mCherry in the whole larva). These data show that the *NK4* reporter is significantly downregulated by Noggin overexpression even when normalized by papilla-specific mCherry levels. p<0.0001 by two-tailed Mann-Whitney. Outliers with GFP value > 80 (5 in control condition) or GFP:mCherry ratio >1.0 (two in the control condition, one in the Noggin condition) were removed from the entire dataset. Complete data with outliers flagged can be found in **Supplemental Data S1.**

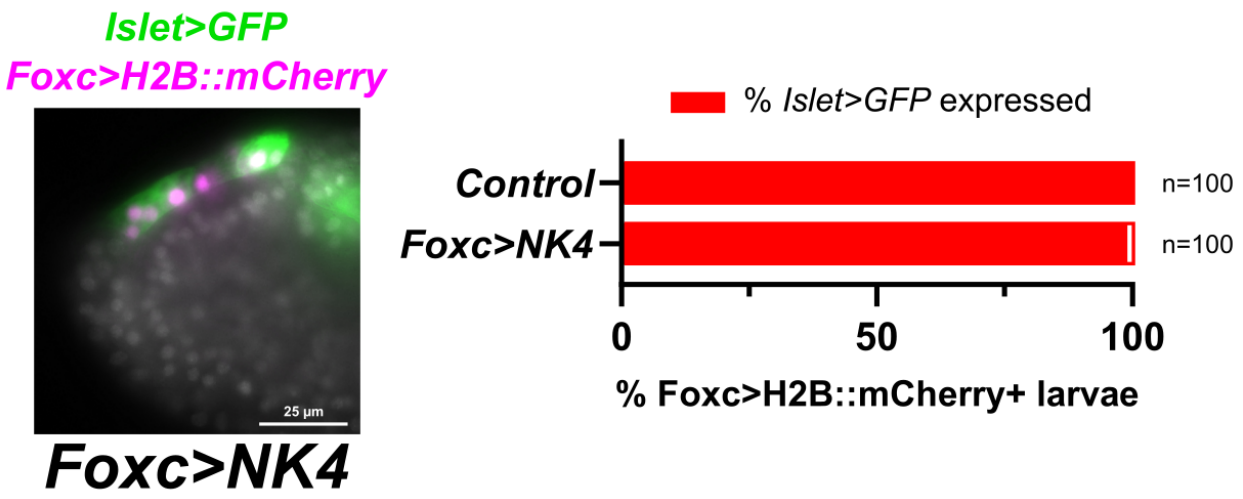

Supplemental Figure S4.

Overexpression of NK4 flattens the papillae but does not abolish *Islet* reporter expression (green) imaged at the larva stage. Larva is counterstained with DAPI (white overlay). *Islet>GFP = Islet intron 1a + bpFOG>Unc-76::GFP.*

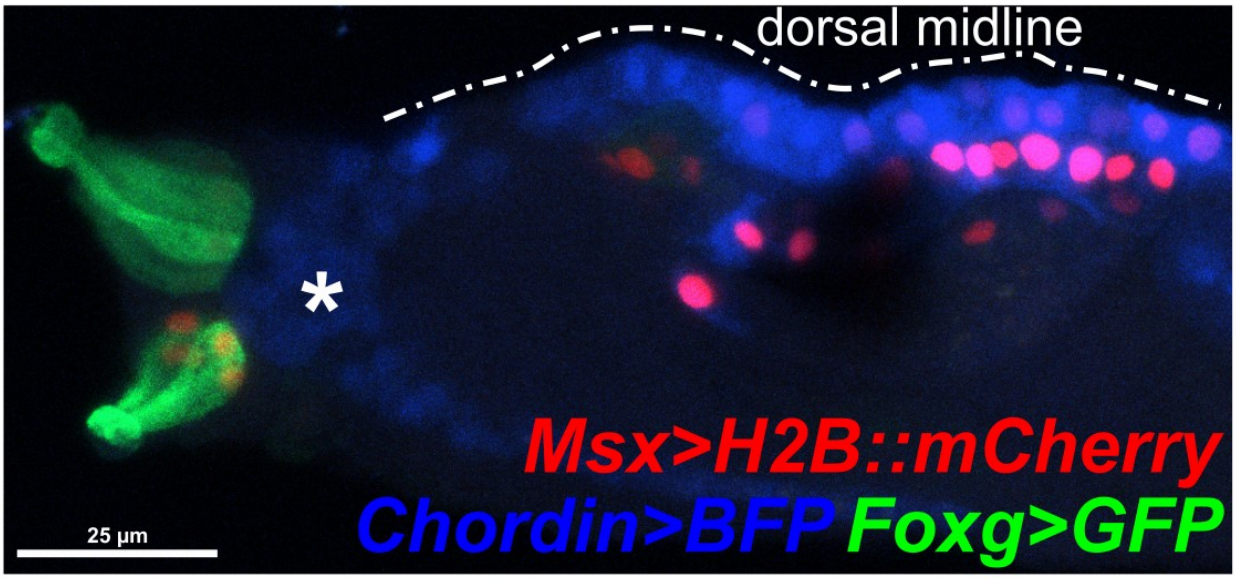

Supplemental Figure S5.

Triple-color image of the same larva imaged in main Figure 7D, here including also *Msx>H2B::mCherry* (red) which labels the ventral but not dorsal papillae. *Msx* reporter expression can also be seen in the dorsal midline. Asterisk denotes Chordin+ migratory mesenchyme cells. BFP = TagBFP; GFP = Unc-76::GFP.

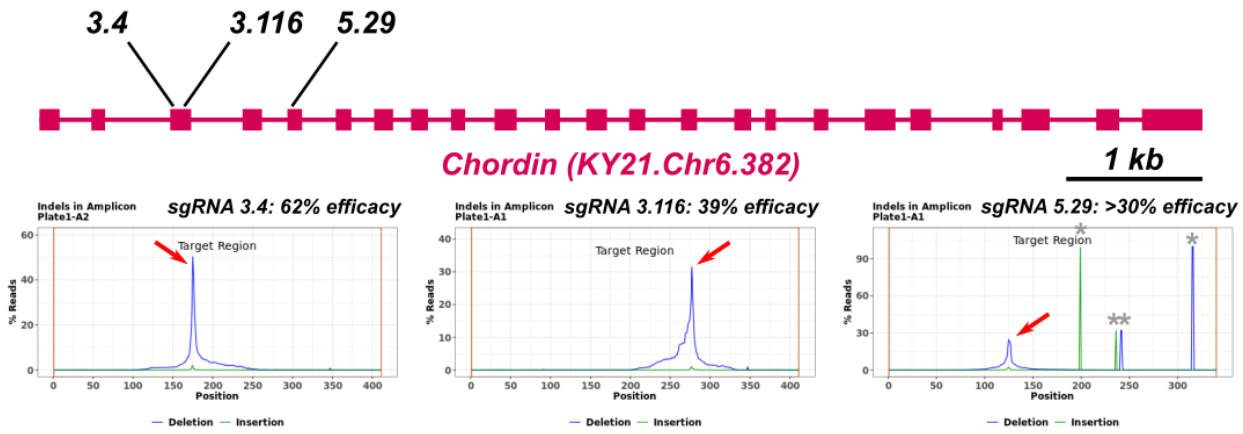

Supplemental Figure S6.

Validation of three sgRNAs targeting *Chordin,* following the protocol in Popsuj et al. 2024 and at: dx.doi.org/10.17504/protocols.io.14egnr97yl5d/v1

Red arrows indicate CRISPR-generated indel peaks. The validation estimate for sgRNA 5.29 is not precise due to the presence of naturally-occurring indels (grey asterisks) in the amplicon sequence.

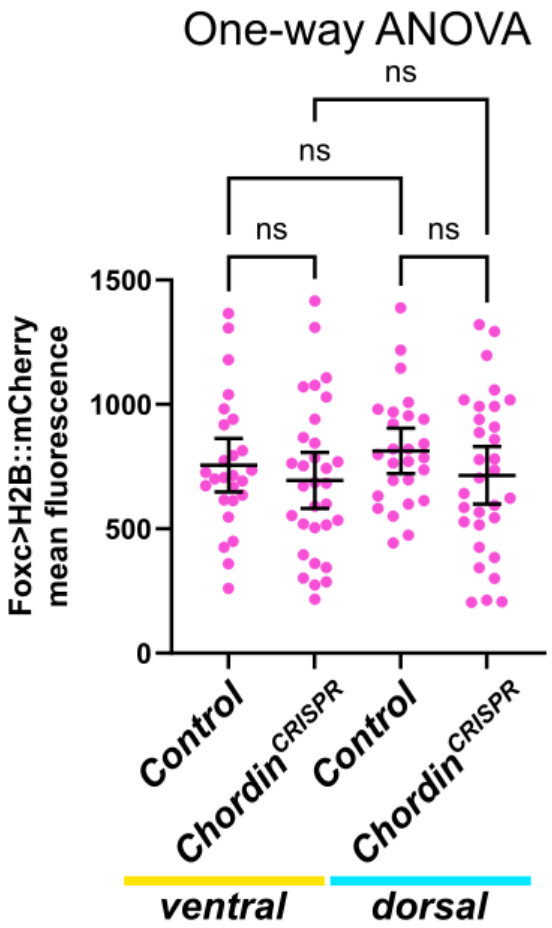

Supplemental Figure S7.

Quantification of *Foxc>H2B::mCherry* mean fluorescence in negative control vs. *Chordin* CRISPR larvae, subdivided by ventral or dorsal papilla territories. These are the mean fluorescence values for mCherry underlying the ratios plotted in main Figure 7H. The mean fluorescence values are not significantly different between the different halves and/or conditions, suggesting the differences observed with the ratios of GFP to mCherry mean fluorescence were indeed attributed to changes in *NK4>GFP* expression. See underlying raw data in **Supplemental Data S1.**

```
                                                  Homeodomain
Msx.Cirobu      HKPNRKPRTPFSTEQLLSLERRFQDKQYLSIAERAEFSASLALSETQVKIWFQNRRAKAKRLHEAEFEK
NK4.Cirobu      HRTRRKPRVLFSQAQVFELERRFKQQRYLSAPEREHLAQILKLTSTQVKIWFQNRRYKCKRMRQDKTLE
NKX2-5.Hosapi   ARRRRKPRVLFSQAQVYELERRFKQQRYLSAPERDQLASVLKLTSTQVKIWFQNRRYKCKRQRQDQTLE
                 : .****. **  *: .*****::::***  ** .::  * *:.*********** *.** :: :  :
```

Supplemental Figure S8.

CLUSTAL O(1.2.4) multiple sequence alignment of the homeodomain of *Ciona robusta* (“Cirobu”) Msx, NK4, and Homo sapiens (“Hosapi”) NKX2-5, showing the conserved KR motif mediating homodimerization of NKX2-5. See **Supplemental Sequences** file for full protein sequences.

906 **Supplemental Video descriptions:**

907

908 **Video S1.**

909 3D projection of confocal image Z-stack through a larva co-electroporated with *NK4 int1.1* +
910 *bpFOG>GFP* (green) and *Foxg>H2B::mCherry* (magenta). Ventral medial papilla on the left,
911 dorsal to the upper right.

912

913 **Video S2.**

914 A Z-stack series from confocal imaging of an *NK4* CRISPR larva (using *Foxc>Cas9::Geminin*$^{N-}$
915 ^{terminus}), co-electroporated with *Seldom>Unc-76::GFP* (green cytoplasm) and
916 *Foxc>H2B::mCherry* (red nuclei). Apical cilia are labeled by immunostaining for acetylated
917 tubulin (AlexaFluor-488, also green), showing that PNs surrounding the single large papilla are
918 still ciliated. Larva is counterstained with DAPI (blue). Anterior to upper left, dorsal on top.

919

920 **Video S3.**

921 3D projection of same larva as in Video S2.

922

923 **Video S4.**

924 3D projection of a confocal image stack through a negative control larva electroporated with
925 Seldom>Unc-76::GFP (green cytoplasm) and Foxc>H2B::mCherry (red nuclei). Apical cilia are
926 labeled by immunostaining for acetylated tubulin (AlexaFluor-488, also green). Larva is
927 counterstained with DAPI (blue). Anterior to bottom right, ventral on left.

928

929

930

931

932

933

934

935

936

937

938

939

940 **REFERENCES**

941 Abitua, P.B., Gainous, T.B., Kaczmarczyk, A.N., Winchell, C.J., Hudson, C., Kamata, K., Nakagawa, M.,
942 Tsuda, M., Kusakabe, T.G., Levine, M., 2015. The pre-vertebrate origins of neurogenic placodes. Nature.
943 Akazawa, H., Komuro, I., 2005. Cardiac transcription factor Csx/Nkx2-5: Its role in cardiac development
944 and diseases. Pharmacology & therapeutics 107, 252-268.
945 Anselmi, C., Sepe, R.M., Manni, L., Sordino, P., 2025. Tunicates in evolutionary developmental biology.
946 Frontiers Media SA, p. 1549081.
947 Berrill, N.J., 1930. Studies in tunicate development. Part I. - General physiology development of simple
948 Ascidians. Philosophical Transactions of the Royal Society of London. Series B, Containing Papers of a
949 Biological Character 218, 37-78.
950 Campbell, M.E.M., Palfreyman, J.W., Preston, C.M., 1984. Identification of herpes simplex virus DNA
951 sequences which encode a trans-acting polypeptide responsible for stimulation of immediate early
952 transcription. J Mol Biol 180, 1-19.
953 Choi, C.Y., Lee, Y.M., Kim, Y.H., Park, T., Jeon, B.H., Schulz, R.A., Kim, Y., 1999. The homeodomain
954 transcription factor NK-4 acts as either a transcriptional activator or repressor and interacts with the
955 p300 coactivator and the Groucho corepressor. Journal of Biological Chemistry 274, 31543-31552.
956 Christiaen, L., Stolfi, A., Levine, M., 2010. BMP signaling coordinates gene expression and cell migration
957 during precardiac mesoderm development. Developmental Biology 340, 179-187.
958 Christiaen, L., Wagner, E., Shi, W., Levine, M., 2009a. Electroporation of transgenic DNAs in the sea
959 squirt Ciona. Cold Spring Harbor Protocols 2009, pdb. prot5345.
960 Christiaen, L., Wagner, E., Shi, W., Levine, M., 2009b. Isolation of sea squirt (Ciona) gametes,
961 fertilization, dechorionation, and development. Cold Spring Harbor Protocols 2009, pdb. prot5344.
962 Cloney, R.A., 1977. Larval adhesive organs and metamorphosis in ascidians: I. Fine structure of the
963 everting papillae of Distaplia occidentalis. Cell and Tissue Research 183, 423-444.
964 Concordet, J.-P., Haeussler, M., 2018. CRISPOR: intuitive guide selection for CRISPR/Cas9 genome editing
965 experiments and screens. Nucleic Acids Research 46, W242-W245.
966 Dolcemascolo, G., Pennati, R., De Bernardi, F., Damiani, F., Gianguzza, M., 2009. Ultrastructural
967 comparative analysis on the adhesive papillae of the swimming larvae of three ascidian species.
968 Invertebrate Survival Journal 6, S77-S86.
969 Dynes, J.L., Ngai, J., 1998. Pathfinding of olfactory neuron axons to stereotyped glomerular targets
970 revealed by dynamic imaging in living zebrafish embryos. Neuron 20, 1081-1091.
971 Feinberg, S., Roure, A., Piron, J., Darras, S., 2019. Antero-posterior ectoderm patterning by canonical
972 Wnt signaling during ascidian development. PLoS genetics 15, e1008054.
973 Fisher, A.L., Ohsako, S., Caudy, M., 1996. The WRPW motif of the hairy-related basic helix-loop-helix
974 repressor proteins acts as a 4-amino-acid transcription repression and protein-protein interaction
975 domain. Molecular and cellular biology 16, 2670-2677.
976 Gandhi, S., Haeussler, M., Razy-Krajka, F., Christiaen, L., Stolfi, A., 2017. Evaluation and rational design of
977 guide RNAs for efficient CRISPR/Cas9-mediated mutagenesis in Ciona. Developmental biology 425, 8-20.
978 Gibboney, S., Orvis, J., Kim, K., Johnson, C.J., Martinez-Feduchi, P., Lowe, E.K., Sharma, S., Stolfi, A., 2020.
979 Effector gene expression underlying neuron subtype-specific traits in the Motor Ganglion of Ciona.
980 Developmental Biology 458, 52-63.
981 Haeussler, M., Schönig, K., Eckert, H., Eschstruth, A., Mianné, J., Renaud, J.-B., Schneider-Maunoury, S.,
982 Shkumatava, A., Teboul, L., Kent, J., 2016. Evaluation of off-target and on-target scoring algorithms and
983 integration into the guide RNA selection tool CRISPOR. Genome biology 17, 1-12.
984 Holland, P.W.H., Booth, H.A.F., Bruford, E.A., 2007. Classification and nomenclature of all human
985 homeobox genes. BMC biology 5, 47.

986 Hotta, K., Dauga, D., Manni, L., 2020. The ontology of the anatomy and development of the solitary
987 ascidian Ciona: the swimming larva and its metamorphosis. Scientific Reports 10, 17916.
988 Hoyer, J., Kolar, K., Athira, A., van den Burgh, M., Dondorp, D., Liang, Z., Chatzigeorgiou, M., 2024.
989 Polymodal sensory perception drives robust attachment and metamorphosis of a prevertebrate
990 zooplanktonic larva. Current Biology.
991 Hozumi, A., Totsuka, N.M., Onodera, A., Wang, Y., Hamada, M., Shiraishi, A., Satake, H., Horie, T., Hotta,
992 K., Sasakura, Y., 2025. Stimulatory and inhibitory G-protein signaling relays drive cAMP accumulation for
993 timely metamorphosis in the chordate Ciona. eLife 13, RP99825.
994 Ikeda, T., Matsuoka, T., Satou, Y., 2013. A time delay gene circuit is required for palp formation in the
995 ascidian embryo. Development 140, 4703-4708.
996 Imai, K.S., Hino, K., Yagi, K., Satoh, N., Satou, Y., 2004. Gene expression profiles of transcription factors
997 and signaling molecules in the ascidian embryo: towards a comprehensive understanding of gene
998 networks. Development 131, 4047-4058.
999 Johnson, C.J., Kulkarni, A., Buxton, W.J., Hui, T.Y., Kayastha, A., Khoja, A.A., Leandre, J., Mehta, V.V.,
1000 Ostrowski, L., Pareizs, E.G., Scotto, R.L., Vargas, V., Vellingiri, R.M., Verzino, G., Vohra, R., Wakade, S.C.,
1001 Winkeljohn, V.M., Winkeljohn, V.M., Rotterman, T.M., Stolfi, A., 2023. Using CRISPR/Cas9 to identify
1002 genes required for mechanosensory neuron development and function. Biology Open 12.
1003 Johnson, C.J., Razy-Krajka, F., Stolfi, A., 2020. Expression of smooth muscle-like effectors and core
1004 cardiomyocyte regulators in the contractile papillae of Ciona. EvoDevo 11, 1-18.
1005 Johnson, C.J., Razy-Krajka, F., Zeng, F., Piekarz, K.M., Biliya, S., Rothbächer, U., Stolfi, A., 2024.
1006 Specification of distinct cell types in a sensory-adhesive organ important for metamorphosis in tunicate
1007 larvae. PLoS biology 22, e3002555.
1008 Karaiskou, A., Swalla, B.J., Sasakura, Y., Chambon, J.P., 2015. Metamorphosis in solitary ascidians.
1009 Genesis 53, 34-47.
1010 Kasahara, H., Lee, B., Schott, J.J., Benson, D.W., Seidman, J.G., Seidman, C.E., Izumo, S., 2000. Loss of
1011 function and inhibitory effects of human CSX/NKX2.5 homeoprotein mutations associated with
1012 congenital heart disease. J Clin Invest 106, 299-308.
1013 Kasahara, H., Usheva, A., Ueyama, T., Aoki, H., Horikoshi, N., Izumo, S., 2001. Characterization of Homo-
1014 and Heterodimerization of Cardiac Csx/Nkx2.5 Homeoprotein *. Journal of Biological Chemistry 276,
1015 4570-4580.
1016 Kim, K., Piekarz, K.M., Stolfi, A., 2025. A gene regulatory network for specification and morphogenesis of
1017 a Mauthner Cell homolog in non-vertebrate chordates. Developmental Biology 522, 51-63.
1018 Kim, Y., Nirenberg, M., 1989. Drosophila NK-homeobox genes. Proceedings of the National Academy of
1019 Sciences 86, 7716-7720.
1020 Lemaire, P., 2011. Evolutionary crossroads in developmental biology: the tunicates. Development 138,
1021 2143-2152.
1022 Liu, B., Ren, X., Satou, Y., 2023. BMP signaling is required to form the anterior neural plate border in
1023 ascidian embryos. Development Genes and Evolution, 1-11.
1024 Liu, B., Satou, Y., 2019. Foxg specifies sensory neurons in the anterior neural plate border of the ascidian
1025 embryo. Nature communications 10, 1-10.
1026 Matsunobu, S., Sasakura, Y., 2015. Time course for tail regression during metamorphosis of the ascidian
1027 Ciona intestinalis. Developmental biology 405, 71-81.
1028 Nakayama-Ishimura, A., Chambon, J.-p., Horie, T., Satoh, N., Sasakura, Y., 2009. Delineating
1029 metamorphic pathways in the ascidian Ciona intestinalis. Developmental biology 326, 357-367.
1030 Pennati, A., Jakobi, M., Zeng, F., Ciampa, L., Rothbächer, U., 2024. Optimizing CRISPR/Cas9 approaches
1031 in the polymorphic tunicate Ciona intestinalis. Developmental Biology 510, 31-39.
1032 Pennati, R., Ficetola, G.F., Brunetti, R., Caicci, F., Gasparini, F., Griggio, F., Sato, A., Stach, T., Kaul-
1033 Strehlow, S., Gissi, C., Manni, L., 2015. Morphological Differences between Larvae of the Ciona

1034 intestinalis Species Complex: Hints for a Valid Taxonomic Definition of Distinct Species. PLOS ONE 10,
1035 e0122879.
1036 Popsuj, S., Cohen, L., Ward, S., Lewis, A., Yoshida, S., Herrera, R.A., Cota, C.D., Stolfi, A., 2024.
1037 CRISPR/Cas9 protocols for disrupting gene function in the non-vertebrate chordate Ciona. Integrative
1038 and Comparative Biology 64, 1182-1193.
1039 Rothbächer, U., Bertrand, V., Lamy, C., Lemaire, P., 2007. A combinatorial code of maternal GATA, Ets
1040 and β-catenin-TCF transcription factors specifies and patterns the early ascidian ectoderm. Development
1041 134, 4023-4032.
1042 Roure, A., Chowdhury, R., Darras, S., 2023. Regulation of anterior neurectoderm specification and
1043 differentiation by BMP signaling in ascidians. Development 150.
1044 Roure, A., Chowdhury, R., Darras, S., 2025. Six3/6 acts downstream of canonical Wnt signaling to
1045 regulate anterior neural border-derived sensory organ formation in ascidian embryos. Development,
1046 dev-204927.
1047 Sakamoto, A., Hozumi, A., Shiraishi, A., Satake, H., Horie, T., Sasakura, Y., 2022. The TRP channel PKD2 is
1048 involved in sensing the mechanical stimulus of adhesion for initiating metamorphosis in the chordate
1049 Ciona. Development, Growth & Differentiation 64, 395-408.
1050 Song, M., Yuan, X., Racioppi, C., Leslie, M., Stutt, N., Aleksandrova, A., Christiaen, L., Wilson, M.D., Scott,
1051 I.C., 2022. GATA4/5/6 family transcription factors are conserved determinants of cardiac versus
1052 pharyngeal mesoderm fate. Science Advances 8, eabg0834.
1053 Stolfi, A., Gandhi, S., Salek, F., Christiaen, L., 2014. Tissue-specific genome editing in Ciona embryos by
1054 CRISPR/Cas9. Development 141, 4115-4120.
1055 Stolfi, A., Levine, M., 2011. Neuronal subtype specification in the spinal cord of a protovertebrate.
1056 Development 138, 995-1004.
1057 Thawani, A., Groves, A.K., 2020. Building the Border: Development of the Chordate Neural Plate Border
1058 Region and Its Derivatives. Frontiers in Physiology 11.
1059 Totsuka, N.M., Hotta, K., 2025. Optogenetic activation of primary sensory neurons induces
1060 metamorphosis in Ciona. Developmental Biology.
1061 Tresser, J., Chiba, S., Veeman, M., El-Nachef, D., Newman-Smith, E., Horie, T., Tsuda, M., Smith, W.C.,
1062 2010. doublesex/mab3 related-1 (dmrt1) is essential for development of anterior neural plate
1063 derivatives in Ciona. Development 137, 2197-2203.
1064 Turon, X., 1991. Morphology of the adhesive papillae of some ascidian larvae. Cah. Biol. Mar 32, 295-
1065 309.
1066 Vedurupaka, S., Jadali, B., Johnson, C.J., Stolfi, A., Popsuj, S., 2025. A protocadherin mediates cell-cell
1067 adhesion and integrity of the oral placode in the tunicate Ciona. bioRxiv.
1068 Wagner, E., Levine, M., 2012. FGF signaling establishes the anterior border of the Ciona neural tube.
1069 Development 139, 2351-2359.
1070 Wagner, E., Stolfi, A., Choi, Y.G., Levine, M., 2014. Islet is a key determinant of ascidian palp
1071 morphogenesis. Development 141, 3084-3092.
1072 Wakai, M.K., Nakamura, M.J., Sawai, S., Hotta, K., Oka, K., 2021. Two-Round Ca2+ transient in papillae by
1073 mechanical stimulation induces metamorphosis in the ascidian Ciona intestinalis type A. Proceedings of
1074 the Royal Society B 288, 20203207.
1075 Waki, K., Imai, K.S., Satou, Y., 2015. Genetic pathways for differentiation of the peripheral nervous
1076 system in ascidians. Nature communications 6, 8719.
1077 Zaffran, S., Frasch, M., 2005. The homeodomain of Tinman mediates homo-and heterodimerization of
1078 NK proteins. Biochemical and biophysical research communications 334, 361-369.
1079 Zeng, F., Wunderer, J., Salvenmoser, W., Ederth, T., Rothbächer, U., 2019a. Identifying adhesive
1080 components in a model tunicate. Philosophical Transactions of the Royal Society B 374, 20190197.

1081 Zeng, F., Wunderer, J., Salvenmoser, W., Hess, M.W., Ladurner, P., Rothbächer, U., 2019b. Papillae
1082 revisited and the nature of the adhesive secreting collocytes. Developmental biology 448(2), 183-198.

1083